The Newsletter of the International Association of Sedimentologists

Issue 4, 2021

Dear IAS Members,

In this issue of the Newsletter of the IAS we are delighted to launch the next round of IAS Institutional, MSc Fieldwork, Postgraduate and Postdoctoral Grants. Be sure to get your applications in nice and early so that you are 'ready to go' once we are all allowed back in the field and labs!

We are also delighted to announce the recipient of the R. W. Faas Research Prize 2021.

A final reminder that the reduced rate Early Bird Registration fees for the IMS in Prague will end very soon. See your there!

Stephen Lokier, *General Secretary*

Don't miss out on Early Bird registration for the 35th International Meeting of Sedimentology, Prague 2021

Early Bird registration for the 35th IMS closes on the 7th of May. Don't miss out on the huge savings to be made by registering before this date!. The registration portal can be found on the **conference website**.

As usual, there are significant additional registration fee discounts for IAS Members.

Follow the IAS on Social Media

Follow the IAS on **Facebook**, **Twitter**, **WeChat** and **LinkedIn** to keep up to date with all of the latest news, announcements and happenings.

@sedimentology and IAS沉积学之家

Announcing the recipient of the R. W. Faas Research Prize 2021

We are delighted to announce that the R. W. Faas Research Prize for 2021 has been awarded to Elizabeth Chamberlain of Vanderbilt University.

The Faas Research Prize is awarded in recognition of outstanding work in the field of marine sedimentology and, particularly, research dealing with fine-grained marine and estuarine sediments.

Elizabeth applies luminescence dating to sedimentary archives as a means of testing how rivers move with time and how people have interacted with their landscapes over centuries to millennia. Her current projects address these topics in the Ganges-Brahmaputra Delta of Bangladesh and the Mississippi Delta of the U.S., among others.

Congratulations Elizabeth!

Don't miss out on all that the IAS has to offer - RENEW TODAY!

The IAS is the home of Sedimentology.

We are very proud of our ability to keep our membership fees so much lower than most other professional societies.

IAS membership runs on an annual basis (1st January – 31st December) so, please do be certain to invest 5 minutes to renew your membership for 2021.

You can find a complete list of the benefits of membership of the IAS **website**.

You may also consider becoming a full member for 5 years at a cost of only €100 – effectively getting one year's membership for free. We also offer 'lifelong' membership for just €400.

STUDENT	FULL
STARTING FROM 10€	STARTING FROM 25€ /year
INCLUDED	**INCLUDED**
Annual membership fee	Annual membership fee
Online Sedimentology Online Basin Research Online Special Publications (5+ years)	Online Sedimentology Online Basin Research Online Special Publications (5+ years)
Travel Grants Postgraduate Grants J. McKenzie Field Work Award Conference Sponsorship Request	Post-doctoral Grants Institutional Grants Conference Sponsorship Request
Printed Sedimentology at favourable rates Reduction for IAS Conferences Printed thematic books discounts	Printed Sedimentology at reduced fee Reduction for IAS Conferences Printed thematic books discounts
Special Lecture Tour hosting	Special Lecture Tour hosting
Newsletter Contributed Content Members Directory	Newsletter Contributed Content Members Directory
OPTIONAL	**OPTIONAL**
Printed Sedimentology **+20€** Online Petroleum Geology **+45€** Online + Printed Petroleum Geology **+50€** Friendship Scheme Sponsor **+15€**	Multiple years membership at reduced fee Lifelong membership at reduced fee Printed Sedimentology **+20€**/year Online Petroleum Geology **+45€**/year Online + Printed Petroleum Geology **+50€**/year Friendship Scheme Sponsor **+15€**/year

Check out these terrific free online resources proudly sponsored by the IAS….

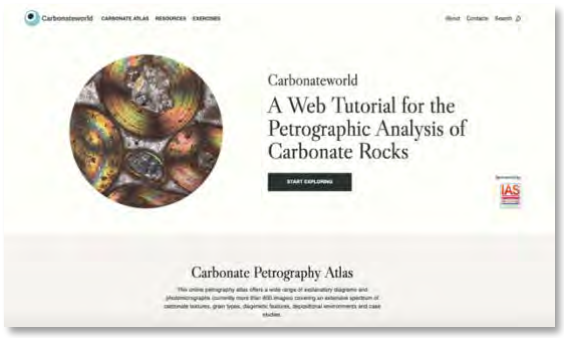

Carbonateworld is an online atlas containing more than 800 images covering an extensive spectrum of carbonate textures, grain types, diagenetic features, depositional environments and case studies. The images are organised in categories and subcategories (e.g., carbonate rock classification, skeletal grains, ooids, corals, burial diagenesis etc.) and are frequently updated with new material.
https://carbonateworld.com/

Seds Online is an free to access online initiative that provides an interactive, adaptable and accessible online platform for anyone with an interest in the field of sedimentology.

Seds Online welcomes members at any career stage, from both industry and academia!

https://sedsonline.com: Twitter @Seds_Online

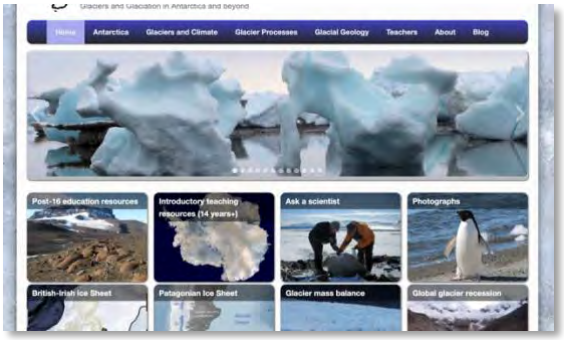

The Antarctic Glaciers website is a fabulous resource for anyone interested in global glacial processes, landforms and sedimentology – despite the name, this site goes way beyond Antarctica!

www.AntarcticGlaciers.org

The IAS still pays the APC for papers accepted in The Depositional Record!

The Depositional Record is a fully open access journal publishing high quality articles from across the field of Sedimentology. The journal covers all timescales, from Ancient to Modern, and welcomes articles that emphasise the application of sedimentary processes to the study of paleoclimate, changes in the chemical environment, ocean acidification, extra-terrestrial sedimentology, and the application of genetic methods to understanding sedimentological processes.

Open Access

Article publication charges are still fully covered by the IAS but this will have to change soon, so submit your paper today!

IAS Regional Correspondents

IAS **Regional Correspondents** are your local hotline to the IAS.

Check out the **News Feed** to see what is happening in your local community. At this link you will also be able to select your correspondent and even elect to receive information from multiple correspondents.

IAS **Regional Correspondents** are IAS Members who have volunteered to act as a representative between sedimentologists in their region and the IAS. If you know of any sedimentology events going on in your region, then please get in touch with your Regional Correspondent and let them know. Similarly, if your region lacks a Regional Correspondent **(see the map here)** and you would like to propose an IAS Member (Full or Student), or yourself, for this position then please send an email to the **General Secretary**.

New Round Now Open – Applications for Institutional Grants (Fall 2021 Session)

Twice a year, IAS awards an **Institutional Grant** of maximum 10,000 Euro, which is intended to support capacity building initiatives in less developed countries (LDCs). Grants will allow earth science departments in LDCs to acquire durable sedimentological equipment for teaching and research, or tools that can be used by all geology students. The grant application should thus clearly demonstrate how the grant will increase the recipient's capacity to teach sedimentology at undergraduate level in a sustainable way.

Applications have to be submitted via the **IAS website**. Application deadline for the Spring 2021 Session is **31st September 24h00 Brussels Time (CEST, UTC+2).**

More information about the Institutional Grant Scheme and guidelines on how to apply can be found on your membership profile.

A message form the organising committee of Tidalites 2021

Dear Friends and Colleagues,
The pandemic-related international emergency is far from going back to normality, as we were optimistically expecting last year. Considering the growing restrictions for international travel and the high risk of potential infection during field trips, and since forecasts do not predict better scenarios for the next early fall, we sadly decided to postpone once again Tidalites to the spring 2022.

The Organising and the Steering Committee have carefully evaluated the possibility to change Tidalites 2021 into a fully virtual conference, as some other international meetings are doing now. However, we strongly want to pursue the chance of a REAL meeting, with in-person presentations, active participation and field trips that, otherwise, could not be replaced by one-hour virtual tours showing through a cold screen the amazing places that would deserve to be 'physically' visited.

However, we are planning some virtual activity for the days of 5-7 October 2021, during which Tidalites 2021 was originally scheduled, such as a series of brief thematic seminars or keynotes, whose details will be announced in the next circulars. Hopefully, this will be a chance to virtually reunite our tidal community in preparation for the conference in Matera.

We all hope to see you all in person in Italy very soon.
On behalf of the Tidalites Organising Committee
Sergio G. Longhitano

New Round Now Open – Applications for Post-Graduate Research Grants (Fall 2021 Session)

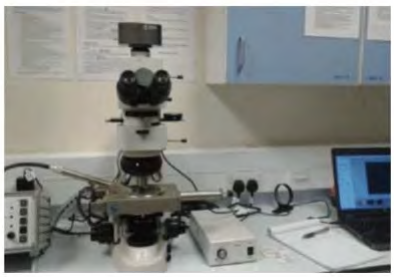

Up to 10 research grants, each to a maximum of €1,000, are awarded twice a year to **IAS Post-Graduate Student Members**. This grant scheme is designed to support PhD students in their studies and research. Post-Graduate Research Grants can be used to (co-)finance fieldwork, acquisition and analysis of data, visits to other institutes to use specialized facilities, etc.
Applications must be submitted via the IAS website. Application deadline for the Fall 2021 Session is **31st September 24h00 Brussels Time (CEST, UTC+2).**
More information about the Post-Graduate Grant Scheme and guidelines on how to apply can be found on your membership profile.

New Round Now Open – Applications for the Judith McKenzie Field Work Award (Fall 2021 Session)

The **Judith McKenzie Field Work Award** aims to promote sedimentological field observations for the newest generation of Earth Scientists – MSc Students.

Up to 5 awards of €300 each, will be awarded twice per year to IAS student members. Since the award is only available for MSc students, proof of student status will be required. The awardee shall also receive a one-year IAS student membership, upon submission of their MSc thesis.

Applicants should apply for the Judith McKenzie Field Work Award via the **IAS website here**. The application requires submission of a grant proposal (written by the student) with budget and CV (template provided on the submission webpage), and a signed letter of recommendation from the student's supervisor.

Application deadline for the Fall 2021 Session is **31st September 24h00 Brussels Time (CEST, UTC+2).**

New Round Now Open – Applications for IAS Post-Doctoral Research Grants (Fall 2021 Session)

IAS Post-Doctoral Research Grants are intended as a seed to a assist Early-Career post-doctoral researchers in either establishing a proof of concept, in order to support applications to national research funding bodies, or to fund areas of a project that were not included in the original project scope.

Up to 4 grants, each to a maximum of €2,500, are awarded twice per year to Early Career IAS members.

The application requires submission of a research proposal with budget and CV (template provided on the **submission webpage**, and a letter of support from the researcher's supervisor, line manager or Head of School. More details about the application procedure can be found on your membership profile.

Application deadline for the Fall 2021 Session is **31st September 24h00 Brussels Time (CEST, UTC+2).**

Eligibility:
· Applicants must be full members of the IAS.
· Applicants must have secured their Ph.D. within the previous 7 years.
· Applicants can only benefit from a Post-Doctoral grant on one occasion.

The Journals of the IAS

For a quick overview of the latest issues of **Sedimentology, Basin Research** and **The Depositional Record**, follow these links:

- **Sedimentology**: directly at Wiley or via the IAS website (after login) for member access
- **Basin Research**: directly at Wiley or via the IAS website (after login) for member access
- **The Depositional Record**: directly at Wiley or via the IAS website

All of the journals of the IAS are active on Twitter. Stay up to date on the latest news and papers in @sedimentology by following the IAS journals: @JSedimentology, @DepositRecord, @BasinResearch.

IAS Grant Reports

The IAS supports postgraduate and post-doctoral researchers via our various grant schemes.

Below you will find some of the latest grant reports received by the IAS.

You can also read recent and past Grant Reports from IAS members who have benefited from Post-Doctoral or Post-Graduate grants here.

IAS POSTDOCTORAL GRANT SCHEME

FINAL SCIENTIFIC REPORT

Project:

Dense shelf water cascades and **sed**iment transport **(DENSED)**

Dr. David Amblas
Dept. of Earth and Ocean Dynamics
Faculty of Earth Sciences, University of Barcelona
C. Martí i Franquès, sn
08028 Barcelona, Spain
damblas@ub.edu

March 2021

1. Introduction

Downslope overflows of dense shelf water (DSW), also known as dense shelf-water cascading (DSWC), are an important atmospheric-driven oceanographic process that occur in certain polar and temperate margins around the world (Fig. 1) (Canals et al., 2006; Ivanov et al., 2004). DSWC events occur seasonally, though at different seasons depending on the setting, and are essential to the formation and ventilation of the deep ocean waters. They therefore contribute to the thermohaline circulation and, by extension, to global climate (Shapiro, 2003). DSWC provides an essential link between shallow and deep waters exchange processes and causes a massive transfer of sediment, organic carbon, and even pollutants and litter in populated areas (Canals et al., 2006; Puig et al., 2008; Ramirez-Llodra et al., 2013; Salvadó et al., 2012). The functioning of deep-sea ecosystems and benthic diversity also seems to be strongly linked to these fluxes (Company et al., 2008; Pusceddu et al., 2012).

Fig. 1. World DSWC observations (red dots). Amblas et al. (in prep), modified from Ivanov et al., (2004) and Canals et al. (2006).

Multiple mechanisms work together to increase the ocean surface waters density to the point that these can sink to abyssal depths. In temperate margins cold and dry winds are the responsible to cool down the continental shelves surface waters and to increase evaporation rates and, thus, the water density. In high-latitudes cold winds are even able to freeze the ocean surface and produce sea-ice that forces out the salt. Once denser than surrounding waters, the cold and salty water sinks to the seafloor, overflows the shelf edge and cascades downslope. During the last decades we have observed a progressive weakening of dense shelf water formation and export in Antarctica (Amblas and Dowdeswell, 2018; Kusahara et al., 2011; Menezes et al., 2017; Snow et al., 2018), which reflects the variability of these complex ice-ocean systems and their vulnerability to climate change. Note that DSW formation in Antarctica is restricted in a few areas with very particular oceanographic, cryospheric and physiographic conditions (Fig. 2). Within this fragile context it is necessary to understand the physical processes involved in the concentration and propagation of DSWC, and to quantify their capacity to erode, transport and deposit sediment.

Field observations show that DSWC can rapidly reshape the seafloor, particularly in submarine canyons (Canals et al., 2006). It has been suggested that DSW fluxes could generate continental slope gullies in Polar Regions too (Dowdeswell et al., 2006; Gales et al., 2021, 2012). In situ near-bottom velocities up to 1.25 $m \cdot s^{-1}$ have been measured for these currents, which are similar to those attained by turbidity currents, although suspended sediment concentrations tend to be very much lower in DSWC, with values of 0.002 to 0.005 $g \cdot l^{-1}$. For this reason, these dilute flows have largely been considered as inefficient pumps of sediment transport, especially when compared with other sediment-laden currents such as turbidity currents (Talling et al., 2013). However, the water volumes

transported by DSWC events are exceptionally large, as these flows can last for days to weeks, or even months in certain polar regions. Hence, we advocate that this fact is enough to reconsider the former assumption.

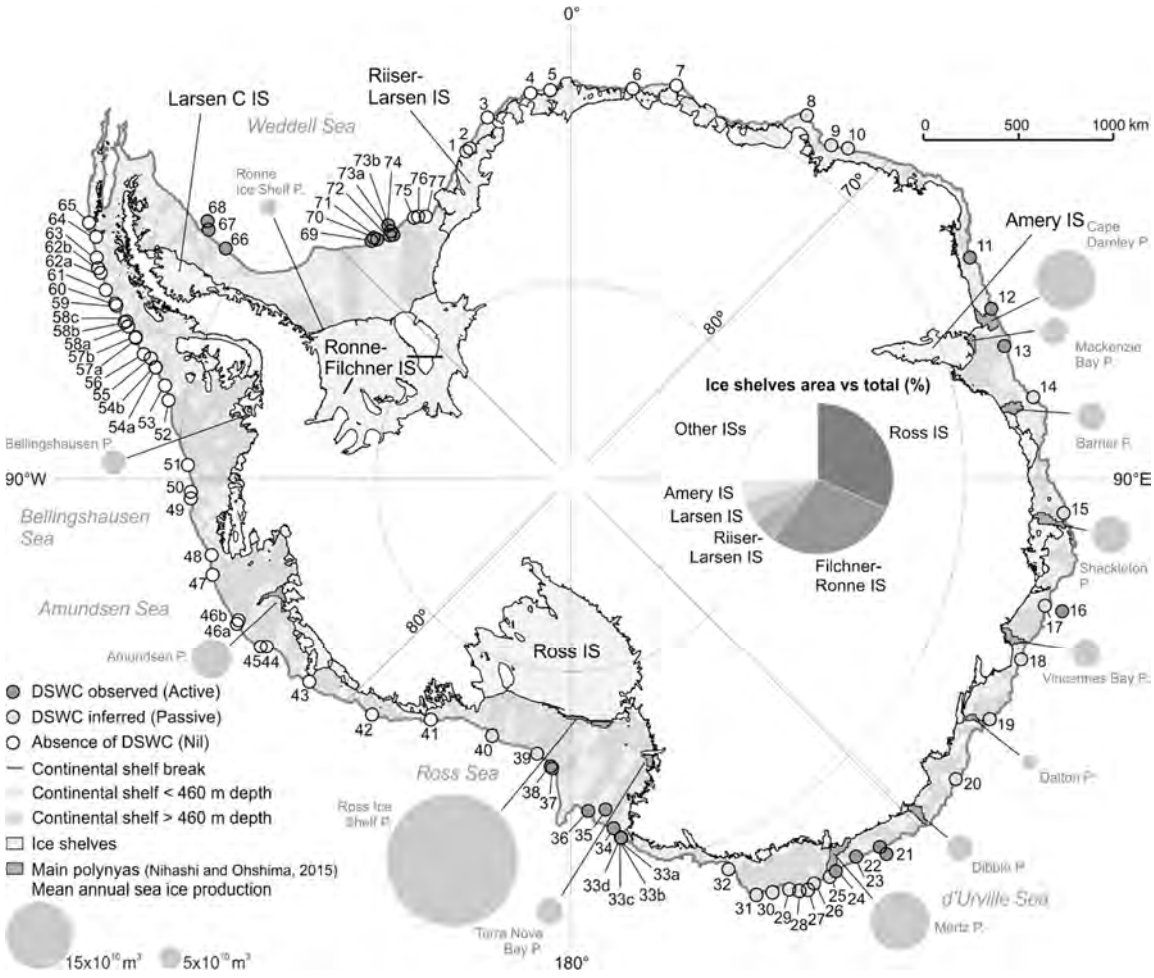

Fig. 2. Location of water column observations showing the presence (dark grey dots) or absence (white dots) of dense shelf-water downslope flows around Antarctica. The coastline and ice shelf areas are derived from the SCAR Antarctic Digital Database. The 460m contour and the continental shelf break are based on IBCSO v. 1.0 (Arndt et al., 2013). The major coastal polynyas and values of mean annual sea ice production are taken from (Nihashi and Ohshima, 2015). The size of the grey circles is proportional to the polynyas sea ice production. The 88 hydrographic observations compiled are all located at or near the shelf break. Confirmed DSW cascade observations are 27 in total and are located in East Antarctica, Ross Sea, East Antarctic Peninsula and Ronne-Filchner. IS is ice shelf; P is polynya. Modified from Amblas and Dowdeswell (2018).

2. Objectives

The DENSED project, awarded by the International Association of Sedimentologists in the 2018 Postdoctoral Grant call, is grounded on two working hypotheses: (i) flow confinement features (coast capes, cross-shelf troughs and canyons) are crucial to concentrate and propagate DSW and, ultimately, to ensure the renewal of the ocean's deep water; and (ii) DSWC are efficient sediment transport mechanisms and it is possible to recognise their modern and past signals on the seafloor geomorphology and in the sedimentary record. These hypotheses are attached to the main DENSED objective: the characterisation of the physical processes involved in the propagation of DSWC and the quantification of its erosion and sediment transport capacity.

3. Explanation of the work carried out and overview of the obtained results

We have tackled the DENSED objective by adapting a process-based depth-integrated numerical model, which was initially developed at IFREMER to simulate turbidity currents. This model, named Nixes-Tc (Jacinto and Burel, 2003), allows to numerically reproduce bottom dense flows and sediment suspensions within different ambient water masses and along complex topographies, and it provides a quantification of the associated transport, erosion and deposition of sediments. To define the model initial and boundary conditions we firstly added new recently published DSWC hydrographic data in Antarctica to the database gathered in the review by Amblas and Dowdeswell (2018) (Fig. 2). For the topography we opted for creating a set of generic terrain models that capture the main morphologic elements observed in glacial margins, where the main volumes of DSW outflows have been reported. This is a wide, deep and landward-sloping continental shelf with crossing troughs, and continental slopes with convex (i.e. canyon) and concave (i.e. trough-mouth fan) shapes. The generic surfaces were created using the software MATLAB by MathWorks. This set up allowed to study the first-order controls of DSW flows concentration and propagation in high-latitude margins, which is giving also important insights to understand the behaviour of DSWC in other geographic settings. The basis for the implementation of the Nixes-TC numerical model to simulate DSWCs was established after two short stays at the Département Géosciences Marines IFREMER (Brest, France) with Dr. Ricardo Silva Jacinto, in February and December 2019.

In Figure 3 we observe the evolution of the modelled DSW overflows during 60 days over an area of 120 x 250 km, based on Ross Sea oceanographic and physiographic data. In Antarctica, the Ross and the Weddell seas are considered to be the main producers of DSW, and hence Antarctic Bottom Water (AABW) (Nihashi and Ohshima, 2015). In addition to large ice shelves and highly productive polynyas, especially in the Ross Sea, both regions exhibit deep and wide continental shelves with large cross-shelf depressions that have the capacity to accumulate and export large volumes of DSW (Amblas and Dowdeswell, 2018) (Fig. 2). The maximum fluxes of DSWC have been measured at the outlets of Ronne-Filchner, in the Weddell Sea (Foldvik et al., 2004), and at the outlet of Drygalski and Joides cross-shelf troughs, in the Ross Sea (Gordon et al., 2004; Muench et al., 2009). During the austral summer/fall season several oceanographic cruises, in different years, registered high DSW outflow speeds over the Ross Sea continental slope (Bergamasco et al., 2002; Gordon et al., 2009, 2004; Jacobs et al., 1985; Muench et al., 2009; Trumbore et al., 1991; Visbeck and Thurnherr, 2009). These studies reported 100 to 250 m thick DSW flows with mean sustained velocities > 0.5 m s^{-1} and flow pulses above 1 m s^{-1}. The initial parameters tested in Fig. 3, based on Ross Sea data, assume a continuous inflow of dense water into the cross-shelf trough, with an horizontal velocity of 0.5 m s^{-1} and a total thickness of 100 m occupying the whole trough width.

Interestingly, active DSWC are observed mostly on the western side of the Ross and Weddell seas due to the action of the Coriolis force (Fig. 2). This observation is also captured in our NixesTC simulation (Fig. 3), which shows a DSW flow strongly deflected to the western side of the cross-shelf trough and continental slope. This is explained both because the high latitude, which increases the Coriolis force magnitude, and the very low density contrast that exists between the DSW flows and the surrounding water. Within this context, the role of the glacial troughs on the continental shelf becomes fundamental, not only to facilitate the accumulation of dense water (Fahrbach et al., 1994; Ivanov et al., 2004), but also to favour its concentration and export towards the shelf edge. This concentration process is considered crucial to give sufficient negative buoyancy to the DSW to reach the lower parts of the continental slope, where it becomes AABW (Baines and Condie, 1998; Ohshima et al., 2013).

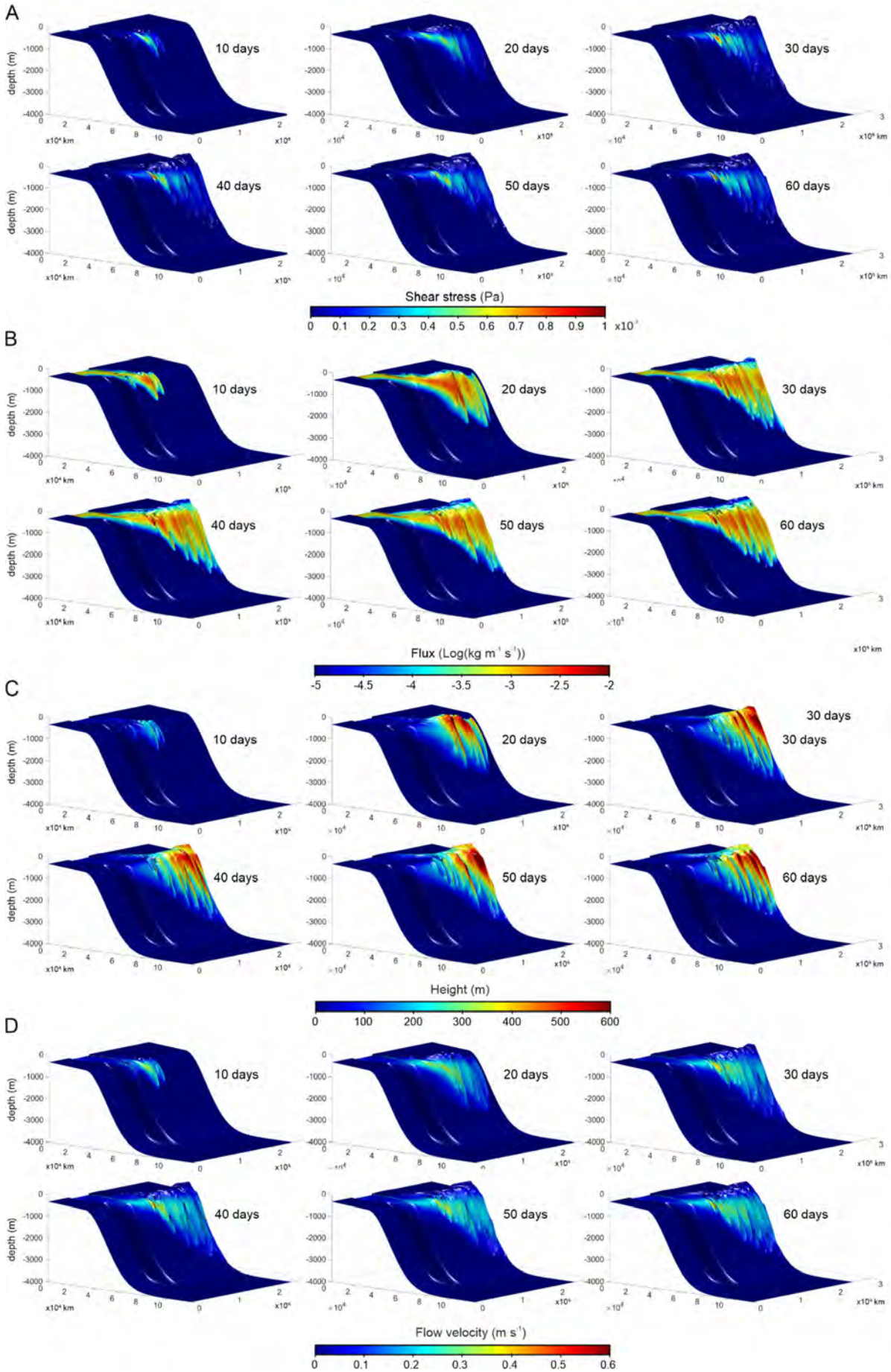
A
10 days
20 days
30 days
40 days
50 days
60 days
depth (m)
Shear stress (Pa)
B
Flux (Log(kg m⁻¹ s⁻¹))
C
Height (m)
D
Flow velocity (m s⁻¹)

Fig. 3. Nixes-Tc modelling results showing the propagation of DSW flows during 60 days over a synthetic terrain model that simulates a typical glacial margin. (a) bed shear stress; (b) sediment flux; (c) flow height; (d) flow velocity. Initial flow conditions have been adopted from Ross Sea (Antarctica) observational mooring data.

Once the DSW flow reaches the shelf edge it starts overflowing and it propagates, also with a remarkable deflection to the west, in a wavy pattern triggered both by the shelf and slope topography, and by the flow evolution itself. This undulating form coincides with the strongly gullied morphology observed in most of the upper slopes of the glaciated margins. Although these small-scale morphologies have been interpreted as relict features developed by energetic turbidity currents during full-glacial conditions (Dowdeswell et al., 2006; Gales et al., 2021, 2012), our results suggest that slope gullies may also be active during interglacial times by the action of DSWC. Maximum bed shear stress, sediment flux and flow velocities are concentrated at the outlet of the cross-shelf trough, on the upper slope (Fig. 3abd), while maximum flow heights are attained in the most distal reaches of the flow in the considered spatial frame (Fig. 3c). The DSW discontinuous period waves that propagate in pulses in the model have also been observed in moorings located along the pathway of DSW overflows in several areas around Antarctica, such as the Ross Sea (Gordon et al., 2009) and the Weddell Sea (Darelius et al., 2009). Shear spikes and plume events, like those observed in the model output, are considered to be key to enhance mixing and entrainment of ambient water masses on the Antarctic continental slope and to ultimately generate AABW (Daae et al., 2019; Foster and Carmack, 1976).

In the next phase of this study we will address the simulation of DSWC over real landscapes in polar and temperate margins. This will allow to study the effect of local physiographic features and small-scale topography to the DSWC propagation, and will provide clues to the potential distribution of its sedimentary deposits.

4. Impact

Our research has the potential to generate interest among researchers in several sub-disciplines given its comprehensive and cross-disciplinary nature. A main contribution of the project has been a better understanding of the physical processes involved in the propagation of DSW flows and their capacity to erode, transport and deposit sediment on continental shelves and slopes. As stated above, we consider that these long-lasting dilute flows can be efficient sediment transport mechanisms in a mid- and long-term point of view and they should be further considered in the classic mass-gravity transport continuum of processes and products, which were formulated more than 70 years ago (Johnson, 1939; Middleton and Hampton, 1976). This can result into improved geomorphic and stratigraphic prediction in these settings, which is highly relevant to understand mixed sediment gravity flows - bottom current systems. The project will also contribute to a better understanding of the past and future effects of climate change on the formation and subsequent impacts of DSWC as well as the recent history of ice cover in polar and subpolar areas.

Different stages of this work have been presented at the 7th International Symposium of Marine Sciences (Barcelona, July 2020 - online) and at the 59th British Sedimentological Research Group Annual General Meeting (Liverpool, December 2020 – online).

References

Amblas, D., Dowdeswell, J.A., 2018. Physiographic influences on dense shelf-water cascading down the Antarctic continental slope. Earth-Science Rev. 185. doi:10.1016/j.earscirev.2018.07.014

Arndt, J.E., Schenke, H.W., Jakobsson, M., Nitsche, F.O., Buys, G., Goleby, B., Rebesco, M., Bohoyo, F., Hong, J., Black, J., Greku, R., Udintsev, G., Barrios, F., 2013. The International Bathymetric Chart of the Southern Ocean (IBCSO) Version 1 . 0 — A new bathymetric compilation covering circum- Antarctic waters 40, 3111–3117. doi:10.1002/grl.50413

Baines, P.G., Condie, S., 1998. Observations and modelling of Antarctic downslope flows: a review. Ocean. ice Atmos. Interact. Antarct. Cont. margin 75, 29–49. doi:10.1029/AR075p0029

Bergamasco, A., Defendi, V., Zambianchi, E., Spezie, G., 2002. Evidence of dense water overflow on the Ross Sea shelf-break. Antarct. Sci. 14, 271–277. doi:10.1017/S0954102002000068

Canals, M., Puig, P., de Madron, X.D., Heussner, S., Palanques, A., Fabres, J., 2006. Flushing submarine canyons. Nature 444, 354–357. doi:10.1038/nature05271

Company, J.B., Puig, P., Sardà, F., Palanques, A., Latasa, M., Scharek, R., 2008. Climate influence on deep sea populations. PLoS One 3. doi:10.1371/journal.pone.0001431

Daae, K., Fer, I., Darelius, E., 2019. Variability and mixing of the Filchner overflow plume on the continental slope, Weddell sea. J. Phys. Oceanogr. 49, 3–20. doi:10.1175/JPO-D-18-0093.1

Darelius, E., Smedsrud, L.H., Østerhus, S., Foldvik, A., Gammelsrød, T., 2009. Structure and variability of the Filchner overflow plume. Tellus, Ser. A Dyn. Meteorol. Oceanogr. 61, 446–464. doi:10.1111/j.1600-0870.2009.00391.x

Dowdeswell, J.A., Evans, J., O'Cofaigh, C., Anderson, J.B., 2006. Morphology and sedimentary processes on the continental slope off Pine Island Bay, Amundsen Sea, West Antarctica. Bull. Geol. Soc. Am. 118, 606–619. doi:10.1130/B25791.1

Fahrbach, E., Peterson, R.G., Rohardt, G., Schlosser, P., Bayer, R., 1994. Suppression of bottom water formation in the southeastern Weddell sea. Deep. Res. Part I 41, 389–411. doi:10.1016/0967-0637(94)90010-8

Foldvik, A., Gammelsrød, T., Østerhus, S., Fahrbach, E., Rohart, G., Schröder, M., Nicholls, K.W., Padman, L., Woodgate, R.A., 2004. Ice shelf water overflow and bottom water formation in the southern Weddell Sea. J. Geophys. Res. 109, doi:10.1029/2003JC002008. doi:10.1029/2003JC002008

Foster, T.D., Carmack, E.C., 1976. Frontal zone mixing and Antarctic Bottom water formation in the southern Weddell Sea. Deep. Res. Oceanogr. Abstr. 23, 301–317. doi:10.1016/0011-7471(76)90872-X

Gales, J., Rebesco, M., De Santis, L., Bergamasco, A., Colleoni, F., Kim, S., Accettella, D., Kovacevic, V., Liu, Y., Olivo, E., Colizza, E., Florindo-Lopez, C., Zgur, F., McKay, R., 2021. Role of dense shelf water in the development of Antarctic submarine canyon morphology. Geomorphology 372. doi:10.1016/j.geomorph.2020.107453

Gales, J.A., Larter, R.D., Mitchell, N.C., Hillenbrand, C.D., Sterhus, S., Shoosmith, D.R., 2012. Southern Weddell Sea shelf edge geomorphology: Implications for gully formation by the overflow of high-salinity water. J. Geophys. Res. Earth Surf. 117, 1–11. doi:10.1029/2012JF002357

Gordon, A.L., Orsi, A.H., Muench, R., Huber, B.A., Zambianchi, E., Visbeck, M., 2009. Western Ross Sea continental slope gravity currents. Deep Sea Res. Part II Top. Stud. Oceanogr. 56, 796–817. doi:10.1016/j.dsr2.2008.10.037

Gordon, A.L., Zambianchi, E., Orsi, A., Visbeck, M., Giulivi, C.F., Whitworth, T., Spezie, G., 2004. Energetic plumes over the western Ross Sea continental slope. Geophys. Res. Lett. 31, 5–8. doi:10.1029/2004GL020785

Ivanov, V. V., Shapiro, G.I., Huthnance, J.M., Aleynik, D.L., Golovin, P.N., 2004. Cascades of dense water around the world ocean, Progress in Oceanography. doi:10.1016/j.pocean.2003.12.002

Jacinto, R.S., Burel, D., 2003. Modélisation du devenir à court terme des boues de dragage rejetées par clapage. Rev. Française Génie Civ. 7, 1151–1166. doi:https://doi-org.sire.ub.edu/10.1080/12795119.2003.9692539

Jacobs, S.S., Fairbanks, R.G., Horibe, Y., 1985. Origin and evolution of water masses near the Antarctic continental margin: evidence from H218O/H216O ratios in seawater. Oceanogr. Antarct. Cont. Shelf 43, 59–85. doi:10.1029/AR043

Johnson, D.W., 1939. The origin of submarine canyons: a critical review of hypotheses. Columbia University Press, New York, USA.

Kusahara, K., Hasumi, H., Williams, G.D., 2011. Impact of the Mertz Glacier Tongue calving on dense water formation and export. Nat. Commun. 2, 159. doi:10.1038/ncomms1156

Menezes, V. V., Macdonald, A.M., Schatzman, C., 2017. Accelerated freshening of Antarctic Bottom Water over the last decade in the Southern Indian Ocean. Sci. Adv. 3, 1–10. doi:10.1126/sciadv.1601426

Middleton, G.V., Hampton, M.A., 1976. Subaqueous sediment transport and deposition by sediment gravity flows, in: Stanley, D.J., Swift, D.J.P. (Eds.), Marine Sediment Transport and Environmental Management.

New York, USA, pp. 197–218.
Muench, R.D., Wåhlin, A.K., Özgökmen, T.M., Hallberg, R., Padman, L., 2009. Impacts of bottom corrugations on a dense Antarctic outflow: NW Ross Sea. Geophys. Res. Lett. 36, 1–6. doi:10.1029/2009GL041347
Nihashi, S., Ohshima, K.I., 2015. Circumpolar mapping of antarctic coastal polynyas and landfast sea ice: Relationship and variability. J. Clim. 28, 3650–3670. doi:10.1175/JCLI-D-14-00369.1
Ohshima, K.I., Fukamachi, Y., Williams, G.D., Nihashi, S., Roquet, F., Kitade, Y., Tamura, T., Hirano, D., Herraiz-Borreguero, L., Field, I., Hindell, M., Aoki, S., Wakatsuchi, M., 2013. Antarctic Bottom Water production by intense sea-ice formation in the Cape Darnley polynya. Nat. Geosci. 6, 235–240. doi:10.1038/ngeo1738
Puig, P., Palanques, A., Orange, D.L., Lastras, G., Canals, M., 2008. Dense shelf water cascades and sedimentary furrow formation in the Cap de Creus Canyon, northwestern Mediterranean Sea. Cont. Shelf Res. 28, 2017–2030. doi:10.1016/j.csr.2008.05.002
Pusceddu, A., Mea, M., Canals, M., Heussner, S., Durrieu de Madron, X., Sanchez-Vidal, A., Bianchelli, S., Corinaldesi, C., Dell'Anno, A., Thomsen, L., Danovaro, R., 2012. Deep-sea benthic ecosystem collapse and recovery after an intense Dense Shelf Water Cascading event. Biogeosciences Discuss. 9, 17855–17884. doi:10.5194/bgd-9-17855-2012
Ramirez-Llodra, E., De Mol, B., Company, J.B., Coll, M., Sardà, F., 2013. Effects of natural and anthropogenic processes in the distribution of marine litter in the deep Mediterranean Sea. Prog. Oceanogr. 118, 273–287. doi:10.1016/j.pocean.2013.07.027
Salvadó, J.A., Grimalt, J.O., López, J.F., Palanques, A., Heussner, S., Pasqual, C., Sanchez-Vidal, A., Canals, M., 2012. Role of dense shelf water cascading in the transfer of organochlorine compounds to open marine waters. Environ. Sci. Technol. 46, 2624–2632. doi:10.1021/es2038189
Shapiro, G.I., 2003. Dense water cascading off the continental shelf. J. Geophys. Res. 108, 1–19. doi:10.1029/2002JC001610
Snow, K., Rintoul, S.R., Sloyan, B.M., Hogg, A.M.C., 2018. Change in Dense Shelf Water and Adélie Land Bottom Water Precipitated by Iceberg Calving. Geophys. Res. Lett. 45, 2380–2387. doi:10.1002/2017GL076195
Talling, P.J., Paull, C.K., Piper, D.J.W., 2013. Earth-Science Reviews How are subaqueous sediment density fl ows triggered , what is their internal structure and how does it evolve ? Direct observations from monitoring of active fl ows. Earth Sci. Rev. 125, 244–287. doi:10.1016/j.earscirev.2013.07.005
Trumbore, S.E., Jacobs, S.S., Smethie, W.M., 1991. Chlorofluorocarbon evidence for rapid ventilation of the Ross Sea. Deep Sea Res. Part A, Oceanogr. Res. Pap. 38, 845–870. doi:10.1016/0198-0149(91)90022-8
Visbeck, M., Thurnherr, A.M., 2009. High-resolution velocity and hydrographic observations of the Drygalski Trough gravity plume. Deep Sea Res. Part II Top. Stud. Oceanogr. 56, 835–842. doi:10.1016/j.dsr2.2008.10.029

New Perspectives on the Piperock Signature: Disentangling Primary Ecological Signatures from the Spatio-Temporal Bias of Outcrop

Across the globe, many Cambrian-aged sandstone strata are typified by dense assemblages of vertical trace fossils (Droser, 1991; Figure 1). These strata have been referred to as "piperocks" for at least 150 years (Peach and Horne, 1884), but the mechanisms which lead to the formation and preservation of this ichnofabric are still the subject of intense study (e.g., Davies et al., 2009; McIlroy and Garton, 2009; Desjardins et al., 2010; Fang et al., 2012). Particularly, piperocks are believed to have suffered an apparent decline over the course of the Phanerozoic (Droser, 1991; McIlroy and Garton, 2004).

Figure 1: *Skolithos* piperock in the Zabriskie Quartzite of Eastern California.

Recent work in sedimentology has shown that the stratigraphic timescales archived in outcrops are hugely variable (Miall, 2015; Tipper, 2015) and can—counterintuitively—be as short as just a few days (Miall, 2016; Davies et al., 2019). In order to test whether this variability might explain the secular demise of piperock, I characterized the: 1. Sedimentology; 2. Piperock characteristics; 3. Outcrop properties; and 4. (Stratigraphic) time for piperocks preserved in three regions: California, Scotland, and Northumberland (England).

As with many things in the past year, the pandemic upended my original plans for extensive field work in a Swedish Cambrian formation. As such, I had to settle for strata close to where I live and study. I first investigated Lower Cambrian piperock in eastern California across four localities in the Inyo-White and Nopah Mountains (Figure 2). Despite the August heatwave, field work was very successful. I classified four formations according to the stipulations in the above

paragraph (Figure 5 shows some observations from the Wood Canyon Formation), and the variations in piperock features observed proved central to the development of my thesis.

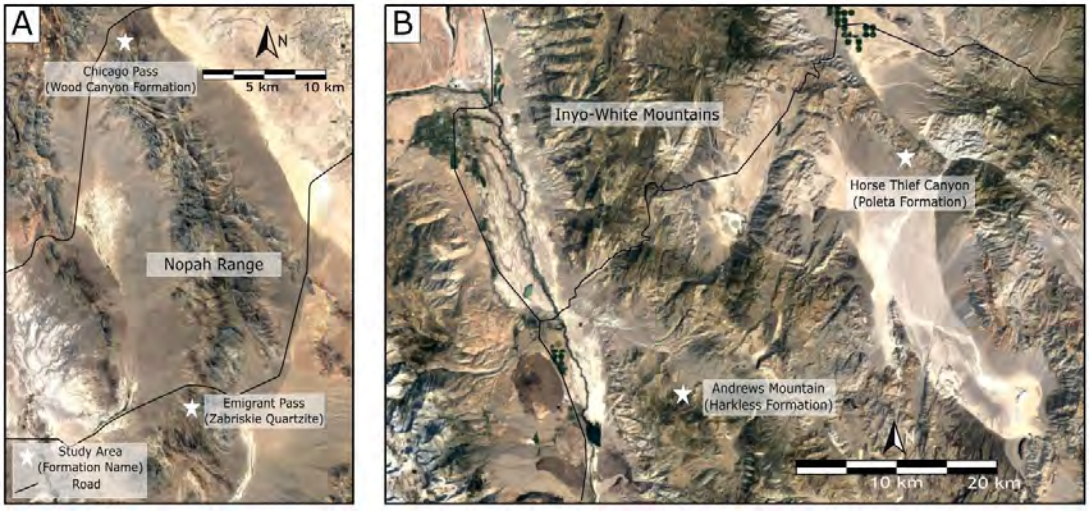

Figure 2: Satellite imagery of the Eastern California study regions. The Nopah Range (**A**) and Inyo Mountains (**B**) regions, showing study localities with the names of outcropping formations. Satellite photos and USGS reports (e.g., Stewart, 1972) show complex and varied structural geology in this region.

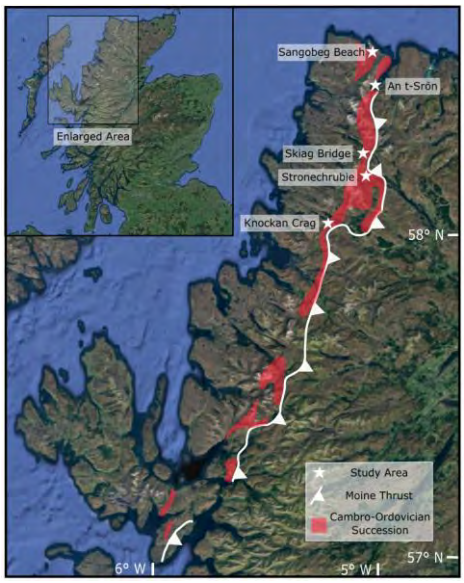

Figure 3: Satellite map of northwest Scotland showing the Moine Thrust, the extent of Cambro-Ordovician exposure, and study localities. Adapted from British Geological Survey Data.

Further field work was undertaken later in the year, this time in northwest Scotland, in part with my supervisor. This largely had the same objectives as the California study (producing a full description of Lower Cambrian piperocks), except that the focus was on rocks of a single formation exposed at multiple localities (Figure 4). This allowed for a more detailed characterization of this formation, which provided an interesting contrast to the varied data collected in California. Further, the contrasting nature of outcrops between the two regions showed the biases that could

be introduced when interpreting piperock with only limited exposure. The piperock observed in Scotland also reached densities of bioturbation much higher than those witnessed in California (Figure 4).

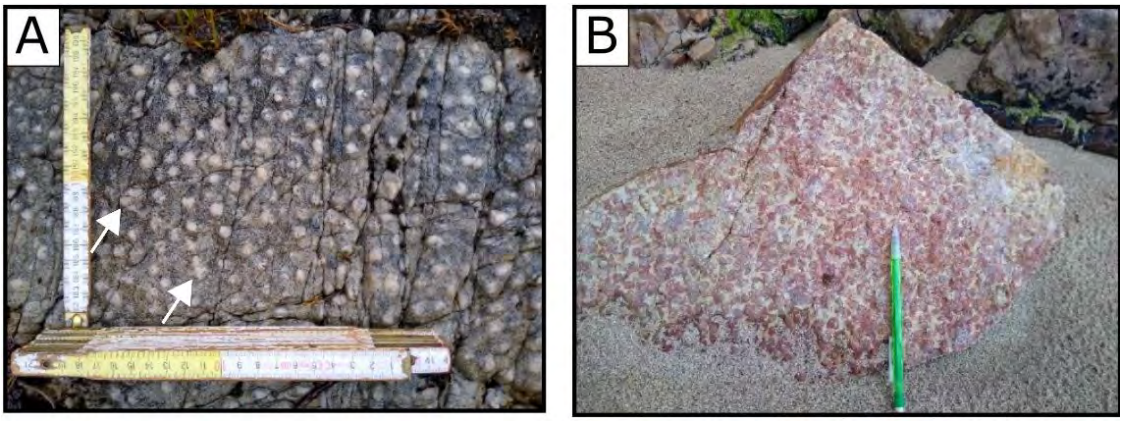

Figure 4: The variability in the expression of bioturbation in the Piperock Member, Eriboll Formation. The size, length, infill, and host lithology of trace fossils varied extensively from outcrop to outcrop. Arrows point to overlapping burrows.

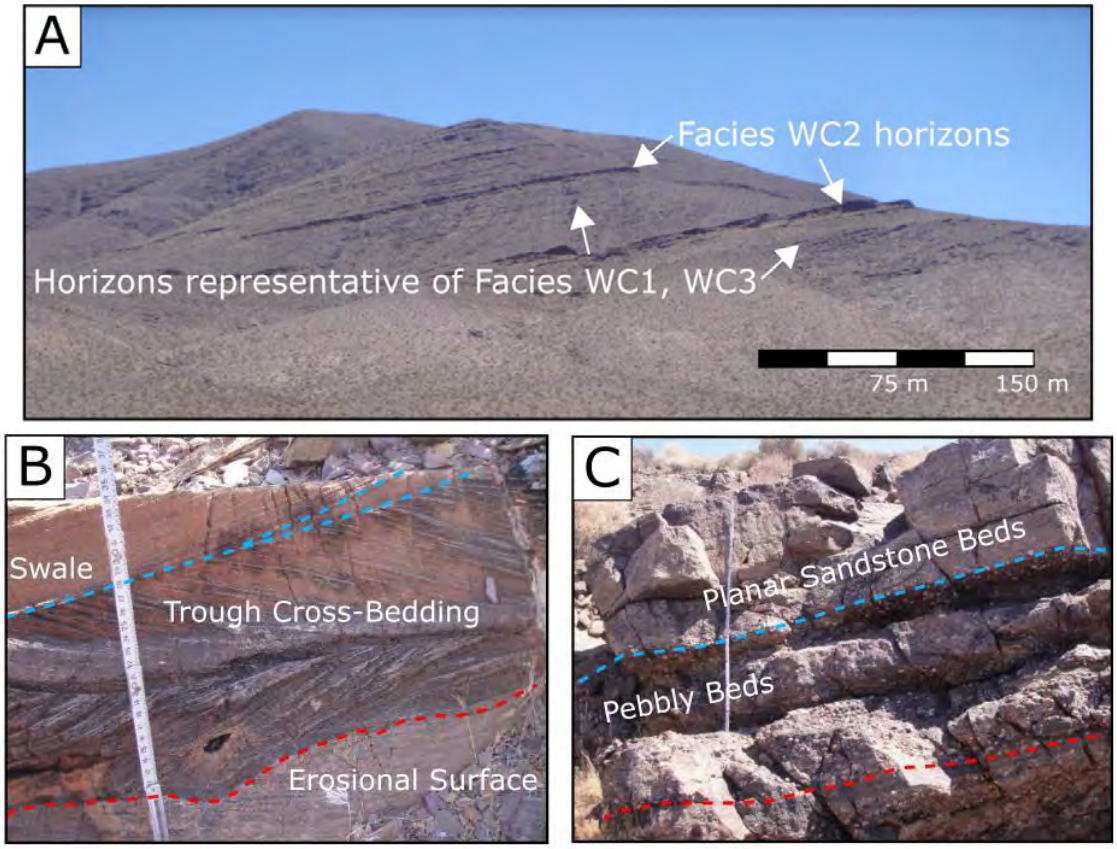

Figure 5: The Wood Canyon Formation of eastern California. **A:** Overview of the primary study area for the formation at Chicago Pass, North Nopah Range. The characterization and description of outcrop properties was a central focus of this project. **B:** Trough cross-bedding, a swale, and an erosional scour in one facies. **C:** Faint planar sandstone beds and pebbly beds in another facies. Erosional surface in red.

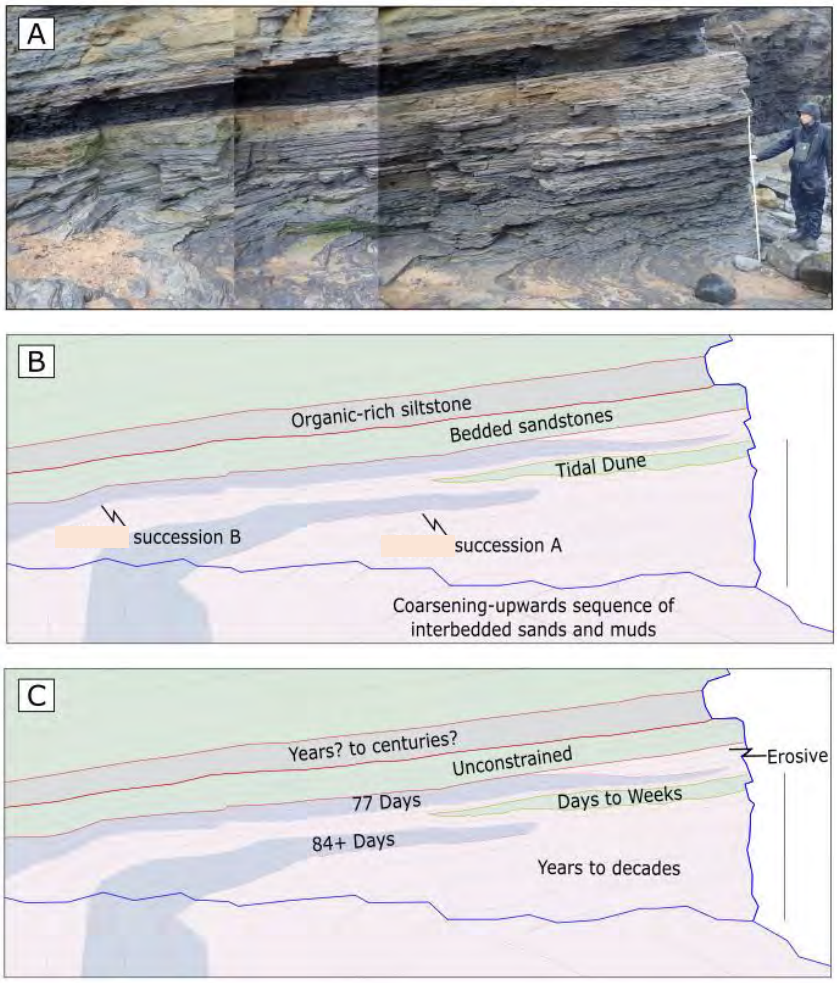

Figure 6: This figure shows the interpretations made of an outcrop which showed a remarkable record of deposition rates. These deposition rates could be compared with the density and spacing of *Skolithos* burrows and could be used to estimate the timescales it took to deposit the outcrop.

These two investigations into Lower Cambrian piperocks were accompanied by a further study in Northumberland (northern England), which investigated piperock preserved in a Carboniferous succession that showed remarkable time resolution. This investigation was key for showing how differential deposition rates might explain the varying expression of piperock at outcrop (Figure 6).

I am immensely grateful to the Judith McKenzie Field Work Award for having supported this project. Work on this thesis gave me the opportunity to conduct independent field work in order to attempt to answer a pervasive question in the field of sedimentology. Even over the short amount of time I was able to spend in the field, I gained confidence in my ability to accurately describe and interpret sedimentary successions. I am certain that I will be able to put these skills to use in future field work, and I hope to be able to further investigate the reasons I suggest in my thesis for the secular demise of piperock.

Palaeoenvironmental analysis of the Katterfeld and Apeleg Fms. (Valanginian – Aptian), Northern Austral Basin, southern Chile (46°S): Insights from major and trace element geochemistry.

Hermann Rivas[1*], Christian Salazar[2], Wolfgang Stinnesbeck[1], Elisabeth Eiche[3]

[1] Institut für Geowissenschaften, Universität Heidelberg, Im Neuenheimer Feld 234, 69120 Heidelberg, Germany
[2] Escuela de Geología, Facultad de Ciencias, Universidad Mayor, San Pío X 2422, 7510041 Providencia, Chile
[3] Institut für Angewandte Geowissenschaften, Karlsruher Institut für Technologie, Adenauerring 20b, 76131 Karlsruhe, Germany
* e-mail: hermann.rivas@geow.uni-heidelberg.de

Introduction

During the Tithonian-Aptian (Upper Jurassic-Lower Cretaceous), a marine incursion spread over a back-arc to intra-arc basin in northern Patagonia (43°-49°s), known as the Aysén Basin – Río Mayo Embayment, and also regarded as the northern part of the Austral Basin (e.g. Suárez *et al*., 2010). Its development is linked to back-arc extension caused by high-angle subduction, and its sedimentary basin fill comprises a transgressive-regressive sequence conformed by the Coyhaique Group (e.g. Haller & Lapido, 1980; Suárez *et al*., 2005; Mpodozis & Ramos, 2008). The latter consists of three marine formations (from base to top): an early transgressive, calcareous-volcaniclastic unit known as the Toqui Formation (Tithonian-Valanginian (Hauterivian?) which developed in a shallow marine environment. The middle member, named Katterfeld Formation (Valanginian-Hauterivian, Barremian?), is formed by black mudstone and it was settled in an outer shelf environment during the post-rift stage. The regressive stage is represented by shallow-marine and paralic sandstone of the Apeleg Formation (Hauterivian-Aptian) which settled during the basin inversion (e.g. Suárez *et al*., 2010). Even though the palaeoenvironmental conditions during the settling of the Coyhaique Group have been interpreted by several authors (e.g. Ramos, 1976; Suárez *et al*., 1996; Suárez *et al*., 2009), they are tentative and based exclusively on a mesoscale approach. Up to date, there is no whole-rock geochemistry for these rocks available, in particular for the "homogeneous", black mudstone of the Katterfeld Fm. Therefore, the first model regarding the provenance, weathering and redox conditions of the Coyhaique Group, based on its geochemistry, is here proposed.

Material and Methods

A total of 45 rock samples were analysed, gathered from seven outcrops of Coyhaique Group, exposed in the Aysén Region of Southern Chile, in a 30 km radius from the city of Coyhaique (46°S). The samples include massive, fissile black mudstone (21), tuffaceous mudstone (5), calcareous mudstone (4), and tuffaceous sandstone (3), taken from the lower- and upper parts of the Katterfeld Fm., and 12 sandstone samples from the lower- and middle parts of the Apeleg Fm.

Samples were powdered in a vibrating-disc mill (model *Scheibenschwingmühle-TS, Siebtechnik GmbH),* and representative aliquots (appr. 2 g) were directly measured for trace elements using a *PANalytical*

X-Ray fluorescence spectrometer (energy dispersive, EDX). For major elements, 2 g aliquots were heated to 900°C to determine the loss of ignition. Subsequently fused beads were made using a Lithium tetraborate & Lithium metaborate mixture (Spectromelt 110, Alfa Aesar) as flux. The fused beads were measured in a *Bruker AXS* X-Ray fluorescence spectrometer (wavelength dispersive, WDX). In order to test the accuracy of the results, the following certified standards were incorporated during the measurement: USGS Marine Sediment Standard (MAG-1), USGS Glass Mountain Rhyolite (RGM-1), and USGS Devonian Ohio Shale (SDO-1). Measurements were carried out in the Laboratory of Environmental and Raw Materials Analysis (Institute of Applied Geosciences) of the Karlsruhe Institute of Technology, Germany.

The resulting data includes the concentration of major- [wt%] and trace elements [ppm]. For the calculation of the Chemical Index of Alteration (CIA *sensu* Nesbitt & Young, 1982), the [CaO] was corrected for carbonate and apatite (CaO*) content, following the guidelines of McLennan (1993) and Fedo *et al*. (1995). In order to evaluate the possible geochemical anomalies, oxide and elemental concentrations were normalized to the composition of the Upper Continental Crust (UCC *sensu* Rudnick & Gao, 2014), and to the post-Archean Australian Shale (PAAS *sensu* Taylor & McLennan, 1985 *in* Condie, 1993).

Preliminary Results

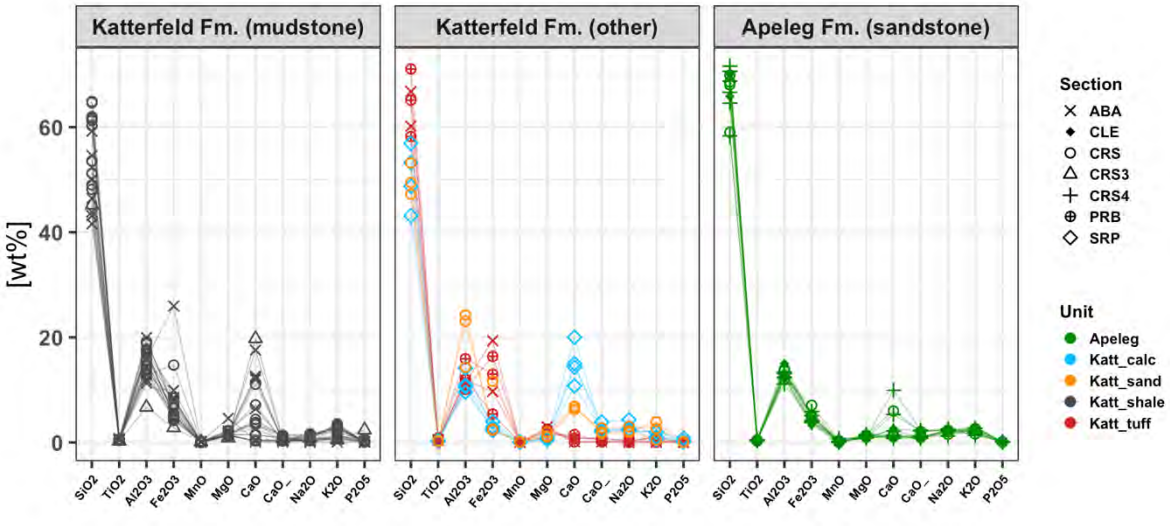

Figure 1. Major elemental composition of the Katterfeld and Apeleg Fms. Section: codes of sedimentary logs here described (several localitites). Unit: Apeleg: samples from the Apeleg Fm.; Katt: samples from the Katterfeld Fm; sandstone: sand; mudstone: calc (calcareous), carbonaceous (shale), tuffaceous (tuff).

Major elements: Samples display a relatively high concentration of SiO_2 (40-70 wt%), followed by Al_2O_3 (10-20 wt%), and Fe_2O_3 (usually <10 wt%; Fig. 1); despite being from different localities, most samples display a similar trend in their major geochemistry (Fig. 1). The geochemistry of most of samples is within the typical range reported for shale, Fe-shale, and wacke (Herron, 1988). Compared

to mudstone, sandstones are richer in SiO_2, tuffaceous mudstone is richer in SiO_2 and Fe_2O_3, and calcareous mudstone has a higher CaO content (Fig. 1). When analyzing the relation of major elements compared to SiO_2 in the whole succession (base to top: Katterfeld – Apeleg Fms.), samples display a negative correlation of Fe_2O_3, MgO, CaO, and P_2O_5; on the contrary, they display a positive correlation of Na_2O and K_2O with SiO_2 (Harker diagrams not presented in this version).

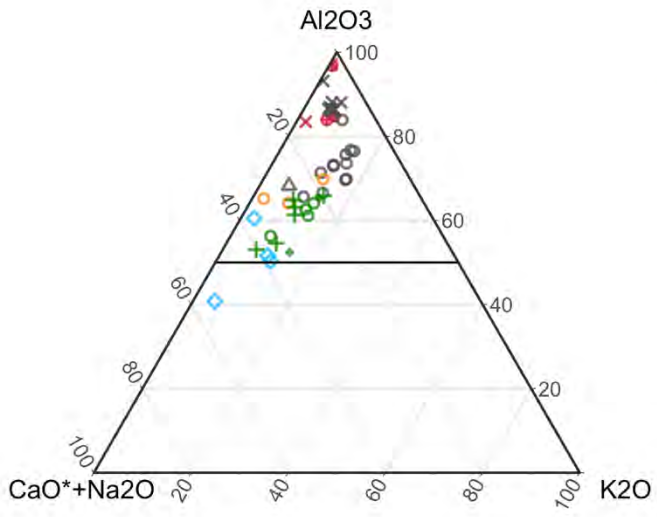

Figure 2*:* A-CN-K ternary diagram (Nesbit & Young, 1982). Values for the Chemical Index of Alteration correlates with the Al2O3 or vertical axis. For explanation of symbology refer to caption of Figure 1.

Regarding the palaeoweathering conditions, basal tuffaceous and carbonaceous mudstone of the Katterfeld Fm. displays the highest CIA values (CIA>80; PRB & ABA sections), suggesting a high degree of weathering of the sediment source; whereas, mudstone of mid- and upper parts of the formation have intermediate values of CIA (between 70-80), similar to the ones for the average shale (Nesbitt & Young, 1982). Upsection, towards the Apeleg Fm., sandstone displays relative low values of CIA (< 70%), reflecting a minor degree of weathering-related alteration (Fig. 2).

Trace elements: Compared to the UCC, mudstone of the Katterfeld Fm. are slightly depleted in Cr, Ni, Rb, Sr, Zr, Nb, Ba, U; and slightly enriched in Zn, As, Y, Mo (Fig. 3). Both sandstone of the Apeleg Fm. and the UCC has a similar trace element geochemistry, however, rocks of the Apeleg Fm. are slightly depleted in Cr, Ni, Sr, Ba, U. Samples from both Katterfeld and Apeleg Fm. display a high enrichment in Cd, likely related to precipitation in reducing environment rich in organic matter (Liu *et al.*, 2017). Trace element composition of calcareous and carbonaceous mudstone is relatively similar, whereas tuffaceous rocks are more variable in composition, showing a marked depletion in Rb, Sr, Ba as well as negative and positive anomalies of Ce, U (Fig. 3).

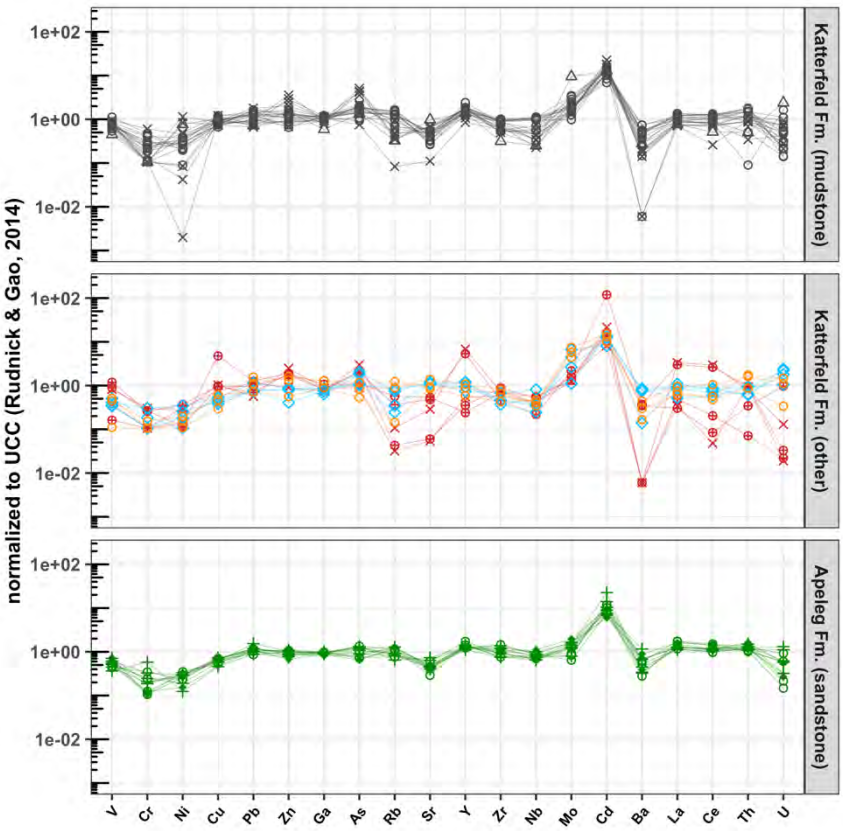

Figure 3: Trace elemental composition, normalized to the Upper Continental Crust (UCC sensu Rudnick & Gao, 2014). For explanation of symbology refer to caption of Figure 1.

References

Condie, K.C. (1993) Chemical composition and evolution of the upper continental crust: Contrasting results from surface samples and shales. *Chemical Geology*, **104**, 1–37.

Fedo, C.M., **Wayne Nesbitt, H.** and **Young, G.M.** (1995) Unraveling the effects of potassium metasomatism in sedimentary rocks and paleosols, with implications for paleoweathering conditions and provenance. *Geology*, **23**, 921–924.

Haller, M.J. and **Lapido, O.R.** (1980) El Mesozoico de la Cordillera Patagónica Central. *Rev. Asoc. Geol. Argentina*, **XXXV**, 230–247.

Liu, Y., **Xiao, T.**, **Perkins, R.B.**, **Zhu, J.**, **Zhu, Z.**, **Xiong, Y.** and **Ning, Z.** (2017) Geogenic cadmium pollution and potential health risks, with emphasis on black shale. *Journal of Geochemical Exploration*, **176**, 42–49.

McLennan, S.M. (1993) Weathering and Global Denudation. *The Journal of Geology*, **101**, 295–303.

Mpodozis, C. and **Ramos, V.A.** (2008) Tectónica jurásica en Argentina y Chile: extensión, subducción oblicua, rifting, deriva y colisiones? *Rev. Asoc. Geol. Argentina*, **63**, 481–497.

Nesbitt, H.W. and **Young, G.M.** (1982) Early Proterozoic climates and plate motions inferred from major element chemistry of lutites. *Nature*, **299**, 715–717.

Ramos, V.A. (1976) Estratigrafía de los lagos La Plata y Fontana, Provincia del Chubut, República Argentina. In: *I Congr. Geol. Chileno, Actas*, Santiago, Chile, 1, 43–64.

Rudnick, R.L. and **Gao, S.** (2014) Composition of the Continental Crust. In: *Treatise on Geochemistry*, *Elsevier*, 1–51.

Suárez, M., **De La Cruz, R.**, **Aguirre-Urreta, B.** and **Fanning, M.** (2009) Relationship between volcanism and marine sedimentation in northern Austral (Aisén) Basin, central Patagonia: Stratigraphic, U–Pb SHRIMP and paleontologic evidence. *J. S. Am. Earth Sci.*, **27**, 309–325.

Suárez, M., **De la Cruz, R.**, **Aguirre-Urreta, M.B.** and **Fanning, M.** (2005) Diachronic Tithonian-Valanginian marine transgression of the Coyhaique Group, Aysén Basin (43°-47°S), Chile. In: *XVI Congr. Geol. Argentino, Actas*, La Plata, Argentina, I, 305–308.

Suárez, M., **De La Cruz, R.** and **Bell, C.M.** (1996) Estratigrafía de la región de Coyhaique (latitud 45°-46° S), Cordillera Patagónica, Chile. In: *XIII Congr. Geol. Argentino y III Congr. Explor. Hidroc., Actas*, I, 575–590.

Suárez, M., **De La Cruz, R.**, **Bell, M.** and **Demant, A.** (2010) Cretaceous slab segmentation in southwestern Gondwana. *Geol. Mag.*, **147**, 193–205.

Taylor, S.R. and **McLennan, S.M.** (1985) The Continental Crust: Its composition and evolution. *Blackwell*, Oxford, 312 pp.

IAS POST-GRADUATE RESEARCH GRANTS REPORT
1st SESSION 2020

Accessing the role of climate-tectonic perturbations in Late Quaternary evolution of terrace sedimentary sequences in Himalayan Frontal Thrust Zone from Northeastern India.

Ms. Aashna Tandon
PhD student, Department of Earth Science, Gujarat University, Ahmedabad, Gujarat, India

INTRODUCTION

The continent-continent collision between the Indian and Eurasian plate (Tibetan plateau) (Figure 1a) around 50 Ma gave rise to the Himalaya, which produced three major fault systems, which runs along-strike length of the Himalayan range, i.e. 1) the northern most Main Central Thrust (MCT), 2) The Main Boundary Thrust (MBT) and 3) the southernmost Himalayan Frontal Thrust (HFT) (Gansser, 1964; Molnar, 1984; Thakur, 2013). The continued convergence and inter-plate tectonics provide ample opportunity to investigate the geomorphic response to ongoing climate and tectonic activity (Lave and Avouac, 2000, 2001; Bookhagen et al., 2005). HFT being the southernmost and youngest among the three major thrusts demarks the sharp tectonic- physiographic boundary between the Siwaliks and Indo-Gangetic plains. The Tertiary Siwaliks are overriding the Quaternary sediments of Indo-Gangetic plains due to thrusting along the HFT (Nakata, 1972).

The northeastern segment of HFT, in particular accounts for higher shortening rates i.e. 21.2 ± 2 mm/yr (Stevens and Avouac, 2015) and one of the highest precipitations in the world. In such environments the sedimentary facies of fluvial terraces reflect the hydrodynamic characteristics as consequence of tectonic/climatic fluctuation during the sediment deposition. The present study extends from the Kameng to Dikrong (Figure 1b) in northeastern Indian Himalayas in the vicinity of the HFT zone with an objective to construct the lithostratigraphy of terrace sequences and to assess the sedimentary response to climate-tectonic pulses.

METHODS:

Lithostratigraphy and Sedimentary Facies Analysis

Owing to covid-19 restrictions in our country, the field work was conducted in the month of January, 2021 with an aim to map and sample the terrace sequences in the entire study area. This field work was mainly focused on to look for exposed outcrops for documenting lithostratigraphic framework and collection of samples for optical dating and geochemistry. Based on physical observation of sedimentary unit, sedimentary structure, nature of contact, grain size and texture, the lithologs were prepared in field. We documented the lithofacies of the terrace sequences in the HFT zone of total 8 rivers from Kameng in the west to Dikrong in the

east. Mapping of sedimentary facies architecture was carried out as it helps in reconstructing the depositional environment, Quaternary lithostratigraphy and palaeohydrological conditions aided with chronology (Miall, 1996).

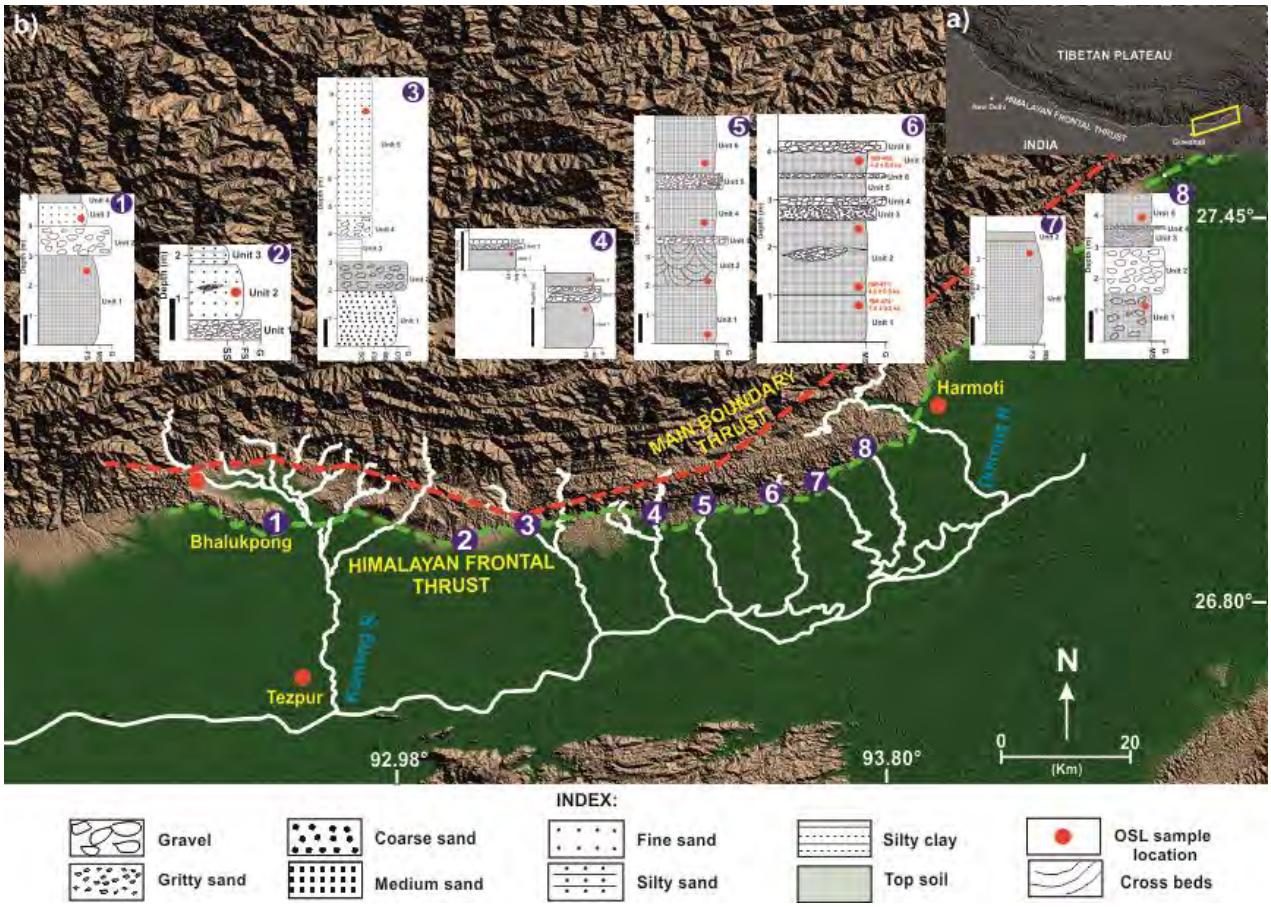

Figure 1: *a) Image shows a simplified map of the Himalayan arc the yellow rectangle shows study area. b) Sites studied at 1. Terrace at Balipara anticline; 2. Bargang River terrace section; 3. Pabhoi Nala terrace section; 4. Burai River terrace section; 5. Tabang river terrace section; 6. Solengi river terrace section; 7. Chengmara River terrace section; 8. Durpang River terrace section)*

OSL Chronology

Luminescence dating relies on the exposure of transported sediment to light prior to deposition and burial of sediment. Total of 18 samples for OSL dating were taken from a freshly exposed fluvial surface in stainless steel pipes. To avoid daylight exposure, standard precautions are taken. In the laboratory, the pipes were opened under subdued red-light conditions and samples from both the end of the pipe, potentially exposed to sunlight during sampling, were removed. The sediments were treated with 1N HCl to digest the carbonates and followed by treatment with H2O2 (30%) to remove organic materials and washed with distilled water in between. The samples were then wet sieved to obtain 90−150 μm grain size fraction. After drying, magnetic grains were removed using Frantz magnetic barrier laboratory separator. The separated fraction was then treated with 40% HF acid for 80 minutes to remove the outer alpha

irradiated skin of the quartz grain upto 25±5 μm with continuous stirring and then treated with 12 N HCL for 30 minutes to remove any precipitated fluorides.

The etched Quartz grains were mounted on stainless steel discs using Silkospray^{TM}. Sample purity was checked by infrared stimulation (IRSL) at room temperature. For every sample a minimum of three natural aliquots were used. All luminescence measurements were carried out using a RisØ TA-DA-15 reader. The detection optics comprises U-340 and BG-39 filters. Beta irradiations were carried out with 25 mCi ^{90}Sr / ^{90}Y source (radiation dose 7.86±62 Gy/minutes). The elemental concentrations of uranium, thorium and potassium will be measured using XRF XEPOS HE spectro at ISR (under maintenance currently).

A conventional Single Aliquot Regeneration (SAR) protocol was used for estimating De. In SAR protocol, OSL measurement of the natural and regeneration doses (L_x) is divided by OSL response to their respective test doses (T_x). The regenerative doses are chosen in such a way that the corresponding sensitivity-corrected luminescence responses (L_x/ T_x) encompass the natural corrected luminescence (L_n/T_n). De is then obtained through interpolation. A pre heat of 240 degree centigrade for 10 seconds was used whereas the cut heat was 200°C for 0 s.

Total 50 aliquots were used for measurement, out of which aliquots yielding (a) recycling ratio <15%, (b) palaeodose error < 15% were considered and the mean of around 12-22 aliquots were taken for the estimation of De. The radial plots were prepared to illustrate the precision on the dose estimates (Galbraith *et al.* 1999). In order to extract the best estimate of the burial dose, statistical models such as the Central Age Model (CAM) of (Galbraith et al., 1999) and the Minimum Age Model (MAM) by Galbraith and Laslett (1993) were employed.

RESULTS

1. Terrace at Balipara anticline:

The fluvial sequence originating from the Balipara anticline shows a 5m thick sequence, which can be divided into 4 units on the basis of sedimentological and facies textural observations. The deposition commences with a sedimentary horizon of 3m thickness of horizontally stratified medium sand horizon at the bottom (Unit 1). This unit is overlain by the gravel bed of 1m (Unit 2) thickness with crude laminations. An 80cm thick layer of fine sand (Unit 3) is sitting on the top of Unit 2 which shows crude laminations. This entire sequence is capped by a 30 cm thick soil cover (Unit 4).

2. Bargang River terrace section:

The fluvial sequence is well exposed at the Bargang River which is in form of ~ 10m incised terrace. On the basis of the sedimentological and facies textural observations, the entire exposed sequence is divided into 5 units. The deposition commences with a sedimentary horizon of 2m thickness of horizontally stratified coarse sand (Unit 1). This is overlain by a 1m thick strata of laminated gravely sand with some scattered gravels (Unit 2). This unit is further succeeded by the ~0.9m thick silty clay sequence (Unit 3) and then with the 0.8m thick fine sand with scattered gravels (Unit 4). This entire sequence is capped by the 5m thick fine laminated sand (Unit 5).

3. Pabhoi River terrace section:

A fluvial sequence of ~2m is well exposed which is divided into 3 units based on physical observation of sedimentary unit, sedimentary structure, nature of contact, grain size and texture, Starting from the bottommost unit of crudely laminated gravel bed (Unit 1) which is 0.5 m in thickness and is further overlain by the fine laminated sand (Unit 2) of 1 m with gravel lens in it. The entire section is covered with sandy silt (Unit 3) of 0.5 m thickness.

4. Burai River terrace section:

The morphostratigraphy of Burai River terrace at the Ramghat of ~2m is well exposed on the right bank of the river with 3 terrace surfaces from youngest i.e. T_0 at the base of sequence (river bed) to T_2 (oldest) at the top. T_0 is the present day river bed. Based on the facies structure and texture, the sequence of T_1 is divided into 3 units. The bottommost layer overlying the T_0 is faintly laminated medium gained sand ($\emptyset$ = 1.11) (Unit 1). Unit 1 is overlain by the 0.4m layer (Unit 2) comprising, horizontally stratified gravel horizon ($\emptyset$ = -0.58) with the sand lens of fine grained sand ($\emptyset$ = 2.09) of 8-10cm in thickness. This sequence is further succeeded by a faintly laminated medium grained sand ($\emptyset$ = 1.6) (Unit 3) making it the T_1 terrace surface.

Palaeobank sequence of ~0.9m being the T_2 terrace surface is also exposed. The sequence is divided into 3 units. The bottommost unit which is overlying the T_1 surface is faintly laminate medium grained sand ($\emptyset$ = 0.56) (Unit 1) of ~0.55m thickness. The Unit 1 is overlain by the 0.12m thick faintly laminated medium grained sand ($\emptyset$ = 1.37) (Unit 2) with scattered gravels. This is further succeeded by the 0.2m thick layer of faintly laminated medium sand ($\emptyset$ =1.14) (Unit 3) making it the T_2 terrace surface (Figure 2 a, b).

5. Tabang River terrace section:

A cliff of ~8m in height is well exposed on right river bank. On the basis of the sedimentary structure and facies textural observations, the entire exposed sequence is divided into 6 units. Starting from the bottommost layer which is overlying the bedrock is of crudely laminated medium grained sand ($\emptyset$ = 1.72) of 2m thickness (Unit 1). The Unit 1 is overlain by 1.5m thickness of cross bedded medium sand ($\emptyset$ = 1.13) (Unit 2). This sequence is further sheeted with a horizontal gravel horizon (Unit 3) of 0.2-0.3m thickness. The Unit 3 is further succeeded with 1.5m thick faintly laminated medium sand ($\emptyset$ = 1.17) (Unit 4). A faintly laminated medium sand layer (($\emptyset$ = 0.35) with scattered gravels (Unit 5) of 0.5m thickness is lying on the top of Unit 4. The top of this sequence overlying Unit 5 is of 2m thick crudely laminated medium sand ($\emptyset$ = 1.26) (Unit 6) (Figure 2c).

6. Solengi River terrace section:

The Solengi River section shows >4m of well exposed fresh section of incised meander having 4 terrace surfaces from youngest i.e. T_0 at the base of sequence to T_3 (oldest) at the top. T_0 at 149 m a.s.l being the present-day river bed. The bottom-most sedimentary sequence i.e. T_1 comprising

faintly laminated sand (Ø = 1.05) (Unit 1) of 1m which overlies on the T_0. T_1 is overlain by 1.6 m thick crudely laminated medium sized sand (Ø = 0.55) unit with gravel lens (Unit 2), making it T_2 terrace surface. This is followed by the layer of clast supported sand (Ø = -0.02) of approximately 30 cm in thickness (Unit 3). This is further overlain by the gravel bed of ~ 20 cm (Unit 4) and medium sized laminated sand (Ø = 0.65) of ~40cm thickness (Unit 5) consecutively. Unit 5 is overlain by ~10cm of gravel bed (Unit 6) and medium sized laminated sand (Ø = 1.05) layer of ~40-50 cm (Unit 7) making it the T_3 terrace surface. This whole section is overlain by the clast layer of ~20 cm with the scour and fills sedimentary contact with T_3 terrace surface (Figure 2d).

7. Chengmara River terrace section:

A cliff of ~5m in height is well exposed on the right bank of Chengmara River near the mountain front. On the basis of the sedimentary facies observations, the entire sequence is divided into 2 litho units. Starting from the bottommost layer which is 3.7 m in thickness consist of laminated medium-coarse sand (Unit 1) and is further overlain by the top soil (Unit 2).

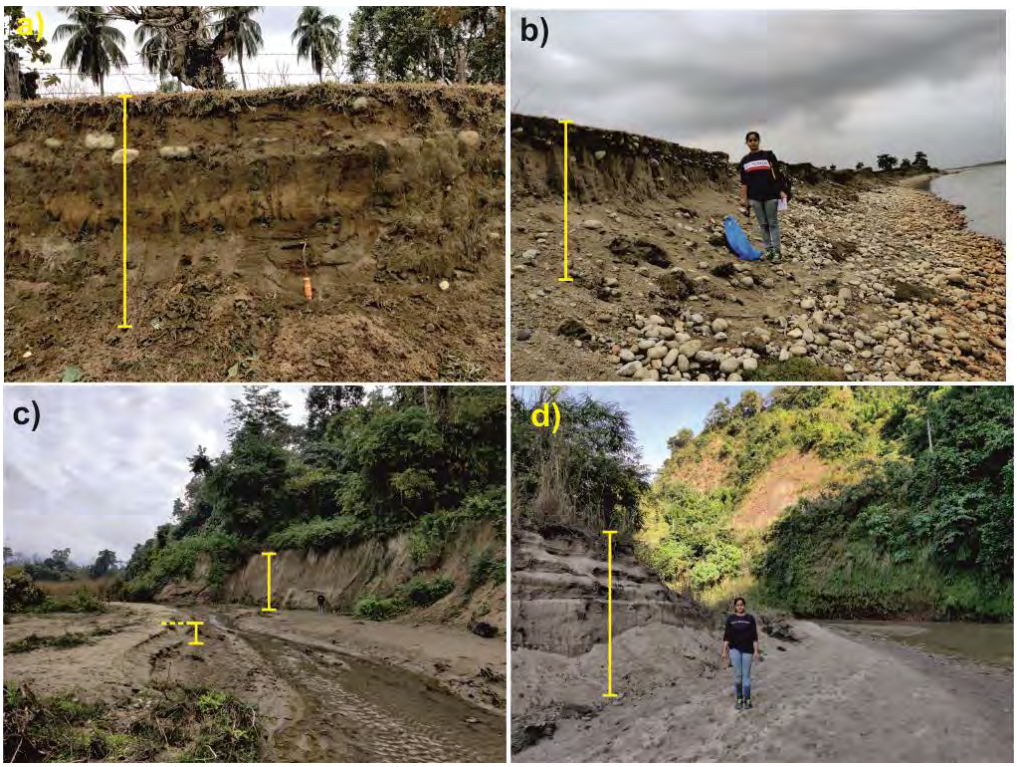

Figure 2: *Field evidences of terrace sequence at: a) Paleobank section on Burai River; b) Terrace section on Burai River; c) Tabang River section; d) Solengi River section.*

8. Durpang River terrace section:

A terrace cliff of ~5m in height is well exposed on the left bank of Durpang River. On the basis of the sedimentary structure and facies textural observations, the entire exposed sequence is divided into 5 units. The bottommost layer of 1.5m in thickness is of crudely laminated medium sand composed of scattered gravels (Unit 1). This sequence is further sheeted with a horizontally

laminated gravel horizon of 1.5m thickness (Unit 2). The Unit 2 is further succeeded by the layer of cross bedded sand of 0.5m thickness (Unit 3). The horizontally laminated granule bed (Unit 4) is capping the Unit 3. A faintly laminated medium sand layer of 1m thickness (Unit 5) is lying at the top of Unit 4.

DISCUSSION AND SUMMARY

Terrace sequences, represents fluvial archives of climatic fluctuations as well as ongoing tectonic activity during the Quaternary period (Bookhagen, et al., 2005; Kumar et al., 2006; Meetei et al., 2007; Singh et al., 2016). Fluvial terraces in the Himalaya have also been studied to investigate the incision rates and its relation with the tectonic uplift (Lave and Avouac, 2000; Wobus et al., 2005; Srivastava and Misra, 2008). The morpho-stratigraphic study along the Kameng River indicates the presence of four levels of alluvial terraces which suggest varying rates of Siwalik uplifts in the Holocene period (Srivastava and Misra, 2008).

The absence of chronology in the NE Himalaya has limited the understanding of behavior of the HFT and neo-deformation of Siwaliks (Srivastava and Misra, 2008). The fluvial terraces carved out in the Siwalik by the rivers crossing the HFT zone shows records of the past events (Figure 2). The terrace configuration in the present study along the mountain front indicates that the river has not been under equilibrium condition during the Holocene and gone through various phases of aggradations and incision.

In Solengi river section in particular, occurrence of different incised cut and fill terraces suggests multiple phases of aggradations and incision. The present study yields the age of T_1 surface, implying the youngest phase of incision takes place after 1.8 ± 0.2 ka. The aggradation of T_2 surface commenced around 4.9 ± 0.5 ka and went through second phase of incision. The sedimentary architecture (gritty sand or granular sand) Unit 3 (base of T_3) with angular and ill sorted nature of granules suggest that this unit got deposited in the hyper-concentrated flow condition (Meetei et al., 2007). Matrix supported gravels with sandy matrix having sub-angular to sub-rounded clast is deposited in a strong debris flow condition (Neemec and Steel, 1984; Monecke et al., 2001). The top of the sequence i.e. T_3 yields a depositional age of 4.8 ± 0.4 ka which indicated the commencement of incisional phase after 4.8 ± 0.4 ka.

The cut and fill terrace sequence at the Burai river correlates with the T_2 terrace configuration shown by Srivastava and Misra (2008) which is characterized by the braided river conditions with one debris flow event embedded in it. Hence, it implies that the aggradation phase started around 8ka and incision commenced <7ka. This suggest that palaeobank sequence adjacent to it got aggraded and incised >8ka. Around 8ka the SW Indian summer monsoon established itself causing higher discharge that leads to incision (Srivastava et al., 2009). The fine laminated sandy unit which occurred at the top of most sequence indicates its aggradation taken place >7ka and deposited under braided channel conditions (Srivastava and Misra, 2008).

The facies deposited in the Durpang River section is in correlation with the T2 terrace sequence along the Sibo River indicating braided channel environment which bracketed the age of its aggradation to be between 10ka – 8ka and incision after 8ka (Srivastava et al., 2009).

The river further experiences aggradation between 8ka and 3ka, when the climate is stable. Various cycles of coarsening upward sequence is indicated in the Unit 1 & Unit 2 of section of Balipara anticline site and similarly in Bargang River section, Burai River section, Tabang River section, and Solengi River section. This suggests the increase in the fluvial energy which may be due to tectonic uplift causing increase in channel gradient and higher precipitation in catchment (Srivastava et al., 2001).

Based on our optical ages we would be in better position to reconstruct climatic and tectonic (uplift) events with precise timing. The De measurements have been made at ISR and all calculations have been completed, however as the XRF of Institute of Seismological Research is under repair (maintenance), the dose rate estimation is remaining, which we plan to do as soon as the machine is repaired.

I thank IAS for assisting my field work which forms important part of my doctoral thesis. Without aid of IAS, I would not have been able to carry out fieldwork at all. I convey my deepest and sincere gratitude for the same.

I also assure I will mention funding support by IAS in future publications from this work and in my doctoral thesis as well, I will send the copy same to IAS as well. Below is the expenditure break up of the field work and attached are the bills of the same for reimbursement.

REFERENCE

- Bookhagen, B., Thiede, R.C. and Strecker, M.R. (2005). Late Quaternary intensified monsoon phases control landscape evolution in the northwest Himalaya. *Geology,* 33, 149-152.
- Galbraith, R.F., Roberts, R.G., Laslett, G.M., Yoshida, H. and Olley, J.M. (1999). Optical dating of single and multiple grains of quartz from Jinmium Rock Shelter, Northern Australia: part I, experimental design and statistical models. *Archaeometry,* 41, 339 - 364.
- Galbraith. R. F. and Laslett, G. M. (1993). Statistical models for mixed fission track ages. *Radiation Measurements,* 21, 459-470.
- Gansser A (1964). The geology of the Himalayas. *Wiley Interscience*, New York, 308.
- Kumar, S., Wesnousky, S.G., Rockwell, T.K., Briggs, R. W., Thakur, V. C. and Jayangondaperumal, R. (2006). Paleoseismic evidence of great surface rupture earthquakes along the Indian Himalaya. *Journal of Geophysical Research,* 111, B03304, 19.
- Lavé, J. and Avouac, J.P. (2000). Active folding of fluvial terraces across the Siwalik Hills, Himalayas of Central Nepal. *Journal of Geophysical Research,* 105, 5735–5770.
- Lavé, J. and Avouac, J. P. (2001). Fluvial incision and tectonic uplift across the Himalayas of central Nepal. *Journal of Geophysical Research,* 106, 26,561–26,591.
- Meetei, Lukram I., Pattanayaka, Sanjay, Bhaskara, Arun, Pandita, M.K. and Tondon, S.K. (2007). Climatic imprints in Quaternary valley fill deposits of the middle Teesta valley, Sikkim Himalaya. *Quaternary International* 159, 32-46.

- Miall, A. D. (1996). The Geology of Fluvial Deposits. *Sedimentary Facies*, Basin Analysis, and Petroleum Geology. 582 pp. Berlin, Heidelberg, New York.
- Molnar, Peter. (1984). Structure and tectonics of the Himalaya: constraints and implications of geophysical data. *Annu. Rev. Earth Planet. Sci*. 12, 489.
- Monecke, K., Winsemann, J. and Hanisch, J. (2001). Climatic response of Quaternary alluvial deposits in the upper Kali Gandali valley (West Nepal). Global and Planetary Change, 28(1): 293-302.
- Nakata, T. (1972). Geomorphic history and crustal movements of the foothills of the Himalayas. *Science Reports, Tohoku University,* 22(7), 39–177.
- Nemec, W. and Steel, R. J. (1984). Alluvial and coastal conglomerates: their significant features and some comments on gravelly mass-flow deposits. In Sedimentology of Gravels and Conglomerates, Koster EH. *Canadian Society of Petroleum Geologists Memoir* Vol. 10; 1–31.
- Singh, A.K., Pattanaik, J. K. and Jaiswal, G. M. K. (2016).Late Quaternary evolution of Tista River terraces in Darjeeling-SikkimTibet wedge: Implications to climate and tectonics. *Quaternary International,* 1-11.
- Srivastava, P., Juyal, N., Singhvi, A.K.and Wasson, R.J. (2001). Luminescence chronology of river adjustment and incision of Quaternary sediments in the alluvial plain of Sabarmati River, north Gujarat, India. *Geomorphology*, 36: 217–229.
- Srivastava, P. and Misra, D.K. (2008). Morpho-sedimentary records of active tectonics at the Kameng river exit, NE Himalaya. *Geomorphology,* 96 (1), 187–198.
- Srivastava, P., Rajak, M.K. and Singh, L.P. (2009). Late Quaternary alluvial fans and paleosols of the Kangra basin, NW Himalaya: Tectonic and paleoclimatic implications. *Catena*, 76(2), 135–154.
- Stevens, V. L., & Avouac, J. P. (2015). Interseismic coupling on the main Himalayan thrust. *Geophysical Research Letters,* 42, 5828–5837.Thakur, V.C. (2013). Active tectonics of Himalayan Frontal Fault System. *International Journal of Earth Science*, 102, 1791-1810.
- Wobus, C., Whipple, K.X., Kirby, E., Snyder, N., Johnson, J., Spyropolou, K., Crosby, B., Sheehan, D. and Willett, S.D. (2005). Tectonics from topography: Procedures, promise, and pitfalls. *Geological Society of America,* 398, 55.

- **DETAILS OF EXPENDITURE:**

Sr. No.	Activity	Amount (INR)	Amount (Euro)
1	Lodging and boarding	38416	436.2
2	Taxi hire for local transport	45495	516.6
Total (Requested from IAS)		**83911**	**952.5**

Geochemical characterization of Pampean aeolian sediments

Renata Coppo[1,2], Diego Gaiero[1,2]

[1]Facultad de Ciencias Exactas, Físicas y Naturales, Universidad Nacional de Córdoba, Argentina
[2]Consejo Nacional de Investigaciones Científicas y Tecnológicas (CONICET) and Centro de Investigaciones en Ciencias de la Tierra (CICTERRA), Universidad Nacional de Córdoba, Argentina

Introduction

Rocks and minerals have different isotope ratios depending, among others, on their geological origin and age of formation. What's more, isotopic compositions are significantly different in the rocks deriving from the mantle and the crust, allowing as a first step a distinction between lithologies with extreme origins. Many authors (e.g., Gousset et al., 1992; Basile et al., 1997; Walter et al., 2000; Delmonte et al., 2004; Gaiero et al., 2007; Grousset and Biscaye, 2005) have demonstrated the importance of the use of radiogenic isotopes (e.g., Sr, Nd, and Pb) when dealing with studies of origin or traceability of aeolian sediments since they maintain and inherit the isotopic composition of the source area of which they derive. Sediments that are deflated or removed by the wind from continental areas become excellent natural tracers of atmospheric circulation because they: a) are transported great distances, b) suffer little chemical modifications during transport and, c) endure in complete climate cycles.

Strontium (Sr) is a divalent alkaline element, having four natural isotopes: ^{84}Sr, ^{86}Sr, ^{87}Sr, and ^{88}Sr. The isotope ^{87}Sr is a radiogenic isotope formed by β- radioactive decay of the ^{87}Rb isotope. The concentration of the ^{87}Sr isotope in a sample depends on the quantity of ^{87}Rb present in the sample, the elapsed time since its formation, and the initial isotopic composition of the Sr in the rock. Since the semi-disintegration period of ^{87}Rb is 4,88 x 10^{10} years, radiogenic ^{87}Sr quantities tend to be very low in samples of low Rb content and are even lower in very young rocks (younger than 50 million years). By convention, reported data referred to the decay system Rb-Sr is referenced using the stable isotope ^{86}Sr.

Neodymium (Nd) is a Rare Earth Element (REE) with chemical properties and ionic radius similar to Samarium (Sm). It has seven natural isotopes: ^{142}Nd, ^{143}Nd, ^{144}Nd, ^{145}Nd, ^{146}Nd, ^{148}Nd, and ^{150}Nd. The isotope ^{143}Nd is a product of α radioactive decay of ^{147}Sm. Data referred to the decay system Sm-Nd are reported as $^{143}Nd/^{144}Nd$. Even though ^{144}Nd is a radioactive isotope, its semi-disintegration period is very long (i.e., 2,38 x 10^{15} years), and hence it is used to reference ^{143}Nd concentrations. Here we present Nd concentrations with the notation ε (epsilon) Nd, which indicates a deviation of the $^{143}Nd/^{144}Nd$ values from present CHUR (Chondritic Uniform Reservoir) values. The CHUR has a value of 0.512638 and is a model that assumes that terrestrial neodymium has evolved from a uniform reservoir whose Sm/Nd ratio is equal to that of the chondrites (Jacobsen y Wasserburg, 1980). Positive εNd(0) values indicate a sample enriched in ^{143}Nd with respect to the CHUR, i.e., derives from a reservoir with a Sm/Nd ratio greater than the chondritic ratio, while negative εNd(0) values indicate that the Nd was originated from a magma with a Sm/Nd ratio lower than that of the CHUR. The case when the εNd(0) value is zero only occurs when the rock or mineral derives from a reservoir with a chondritic Sm/Nd ratio (Faure, 1986).

Lead (Pb) is a heavy metal that contains only four stable isotopes, being ^{204}Pb the only non-radiogenic one. The rest of the Pb isotopes are the final product of the decomposition of three complex uranium (U) and thorium (Th) decay chains. However, the intermediate members of each series have relatively short half-lives. ^{206}Pb is the final decay product of ^{238}U, ^{207}Pb is the decay product of ^{235}U and ^{208}Pb is the decay product of ^{232}Th. The half-life of ^{238}U is comparable to the Earth's age. For ^{235}U, the half-life is much shorter so that all the primordial ^{235}U of the Earth has already decayed to ^{207}Pb. The half-life of ^{232}Th is comparable to the age of the Universe.

Pampean loess represents the most proximal dust deposit to the dust source areas indicated by Gili et al. (2016; 2017), corresponding to the Arid Diagonal of southern South America. By analyzing the isotopic composition expressed in terms of $^{87}Sr/^{86}Sr$, $^{143}Nd/^{144}Nd$, $^{208}Pb/^{204}Pb$, $^{207}Pb/^{204}Pb$, and $^{206}Pb/^{204}Pb$ ratios of the Pampean loess sediments in three different sections (i.d. Lozada, Tortugas, and Gorina), this study aims to determine the isotopic signal of the aeolian sediments. Comparing the results with the geochemical signals of the potential source areas of southern South América, we can obtain an approach of the provenance of the windblown material and determine the atmospheric paleocirculation.

Materials and Methods

The isotopic composition of the sediments, measured in terms of $^{87}Sr/^{86}Sr$, $^{143}Nd/^{144}Nd$, $^{208}Pb/^{204}Pb$, $^{207}Pb/^{204}Pb$ and $^{206}Pb/^{204}Pb$ ratios of 67 loess samples (22 = >44 µm, 22 = <44 µm, 10 =< 5 µm and 12 bulk samples) were analyzed in external laboratories (Laboratorio de Geología Isotópica (LGI) del Instituto de Geociencias de la Universidad Federal de Río Grande do Sul, Brasil.).

100 mg of loess sample were brought into solution by tri-acid attack (HF-HNO3-HCl) using Teflon Savillex containers. Nd and Sr were then analyzed by Thermal Ionization Mass Spectrometry (i.e. Sr and Nd isotopes, TIMS - Thermal Ionisation Multicollector Mass Spectrometry), while Pb ratios were measured using a VG Sector 50-30 mass spectrometer (ICP-MS).

Once in solution, the Sr, Nd and Pb atoms of the samples were chemically separated from the rest of the elements through chromatographic columns following standard techniques (Richard et al., 1976; Pin et al., 1994; Goldstein et al. 2003).

Pb was extracted with HCl using anion exchange chromatographic columns (AG-1 X 8 resin, 100-200 mesh). Pb isotopes were measured using the "double spike $^{207}Pb/^{204}Pb$" technique. The external reproducibility for the $^{206}Pb/^{204}Pb$, $^{207}Pb/^{204}Pb$ and $^{208}Pb/^{204}Pb$ ratios, determined by multiple analyzes using the NBS 981 standard, was 2σ. Control blanks performed with each determination resulted within the expected parameters.

For Sr separation, the samples were purified on 30 µL columns using Eichrom Sr Spec resin and HNO3 3N. Once separated, the residue was deposited on tungsten filaments, and multiple analyzes of the NBS 987 standard were made. The $^{87}Sr/^{86}Sr$ average ratio was 0.710270 ± 13 (2σ of external reproducibility, n = 30), and the samples were corrected to a value of 0.71227. For the Nd obtention, rare earth elements (REE) were separated from other cations using 100 µL columns with TRU-Spec resin and HNO3 1,6N. Then pure Nd was obtained using columns of

800 µL. The residue was deposited in Rhenium filaments and multiple analyzes of the La Jolla standard were made that gave an average for $^{143}Nd/^{144}Nd$ of 0.511859 ± 13 (2σ of external reproducibility, n = 25) and the samples were corrected to a value of 0.511860.

Results

Samples were analyzed in three fractions in order to separate the three grain size populations that are observed in grain size analyses. The purpose of analyzing the geochemical signal for each population is to see if all correspond to the same source.

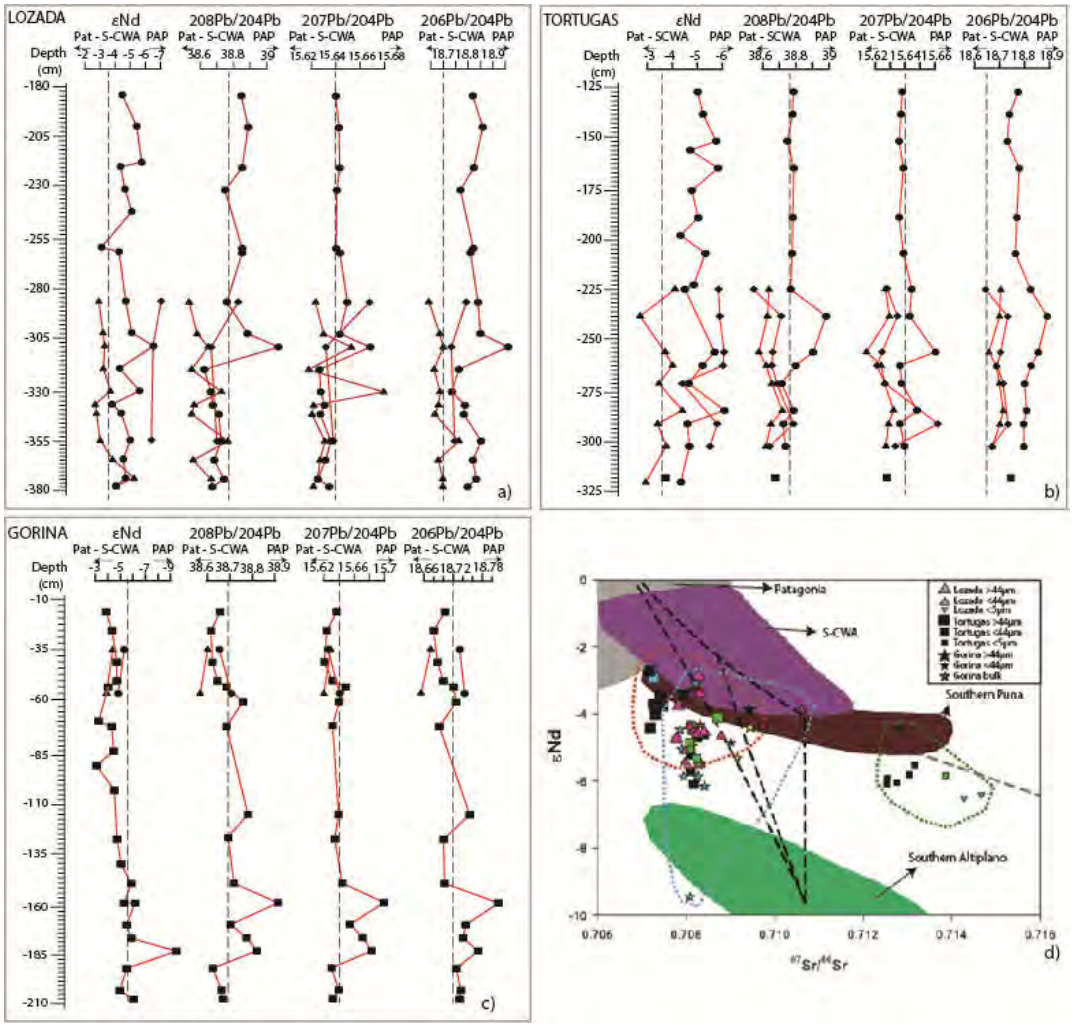

Figure 1. Isotopic composition of a) Lozada, b) Tortugas and c) Gorina in terms of ƐNd, $^{208}Pb/^{204}Pb$, $^{207}Pb/^{204}Pb$ and $^{206}Pb/^{204}Pb$ against depth. Triangles indicate analyses fraction >44µm, circles indicate alanyses fraction <44µm, diamonds indicate analyses fraction <5µm and squares indicate bulk analyses fraction. Figure d) show isotopic composition of loess samples in terms of $^{87}Sr/^{86}Sr$ vs ƐNd compared with previous data of the potential source areas of southern South America. Loess samples have been dated by OSL and are represented according to which MIS (Marine Isotope Stage) correspond.

References

Basile, I., Grousset, F.E., Petit J.R., Biscaye, P.E. and Barkov, N.I. (1997) Patagonian origin of glacial dust deposited in E. Antarctica (Vostok and Dome C) during glacial stages 2, 4 and 6. EPLS. 146, 573-589.

Delmonte, B., et al. (2004).Comparing the Epica and Vostok dust records during the last 220,000 years: stratigraphical correlation and provenance in glacial periods. Earth Planetary Science Letters 66, 63-87.

Faure, G., (1986). Principles Isotope Geology. 2nd ed., Wiley, New York.

Gaiero, D.M., et al. (2007a). A uniform isotopic and chemical signature of dust exported from Patagonia: Rock sources and occurrence in southern environments, Chem. Geol.238, 107-120.

Gili, S., D. M. Gaiero, S. L. Goldstein, F. ChemaleJr, E. Koester, J. Jweda, P. Vallelonga, and M. R. Kaplan (2016), Provenance of dust to Antarctica: A lead isotopic perspective, Geophys. Res. Lett., 43, doi:10.1002/2016GL068244.

Gili, S., D. M. Gaiero, S. L. Goldstein, F. Chemale Jr., J. Jweda, M. R. Kaplan, R. A. Becchio and E. Koester (2017). Glacial/interglacial changes of Southern Hemisphere wind circulation from the geochemistry of South American dust. Earth and Planetary Science Letters.

Goldstein, S. L., & Hemming, S. R. (2003). Long-lived isotopic tracers in oceanography, paleoceanography, and ice-sheet dynamics. Treatise on geochemistry, 6(6), 453-489.

Grousset, F. E., Biscaye, P. E., Revel, M., Petit, J. R., Pye, K., Joussaume, S., & Jouzel, J. (1992). Antarctic (Dome C) ice-core dust at 18 ky BP: Isotopic constraints on origins. Earth and Planetary Science Letters, 111(1), 175-182.

Grousset F.E., Biscaye P. E., 2005. Tracing dust sources and transport patterns using Sr, Nd and Pb isotopes. Chem. Geol. 222, 149-167.

Jacobsen, S. B., & Wasserburg, G. J. (1980). Sm-Nd isotopic evolution of chondrites. Earth and Planetary Science Letters, 50(1), 139-155.

Pin, C., Briot, D., Bassin, C., & Poitrasson, F. (1994). Concomitant separation of strontium and samarium-neodymium for isotopic analysis in silicate samples, based on specific extraction chromatography. Analytica Chimica Acta, 298(2), 209-217.

Richard, P., Shimizu, N., & Allegre, C. J. (1976). 143Nd/146Nd, a natural tracer: an application to oceanic basalts. Earth and Planetary Science Letters, 31(2), 269-278.

Walter, M. R., Veevers, J. J., Calver, C. R., Gorjan, P., & Hill, A. C. (2000). Dating the 840–544 Ma Neoproterozoic interval by isotopes of strontium, carbon, and sulfur in seawater, and some interpretative models. Precambrian Research, 100(1), 371-433.